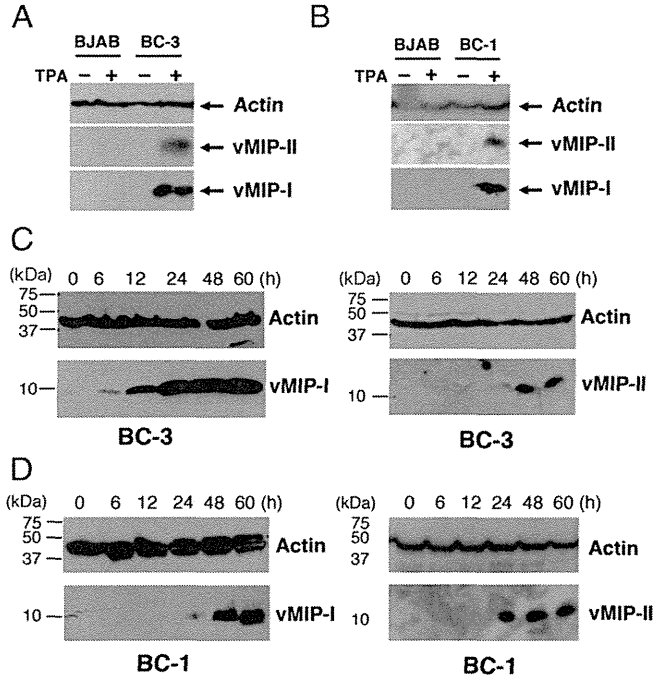

Fig. 3. Detection of vMIP-I and vMIP-II gene products in a KSHV-infected PEL cell line. BC-1 and BC-3 cells were treated with TPA for the indicated number of hours, and the whole-cell extract was prepared after the indicated time post-induction. vMIP-I and vMIP-II were detected by Western blotting and IFA with anti-vMIP-I and -vMIP-II antibodies. Western blot analysis of protein extracted from BC-3 and BJAB cells (A), and BC-1 and BJAB cells (B) with either the anti-vMIP-I or the anti-vMIP-II MAb. Arrows indicate actin, vMIP-I, and vMIP-II proteins. As expected, the estimated sizes of the vMIP-I and vMIP-II proteins, based on comparisons with the migration of molecular size markers, was around 10 kDa. Expression kinetics of vMIP-I (left panel) and vMIP-II (right panel) in TPA-treated BC-3 (C) and BC-1 (D) cells by Western blot analysis. BC-1 and BC-3 cells were harvested after 6, 12, 24, 48, and 60 h post-induction. The lysate was subjected to Western blot analysis as in (A).

GvM1-D3, GvM2-Full, GvM2-D1, GvM2-D2, and GvM2-D3 genes were generated by PCR using the following primer sets: vMIP-I-1F (5′-ATGAATTCCAGATGGCCCCCGTCCAC-3′) and vMIP-I-5R (5′-CCGTGTCGACCGTCTAAGCTATGGCAGGCAGC-3′); vMIP-I-2F (5′-ATGAATTCGCGGGGTCACTCGTGTCG-3′) and vMIP-I-5R; vMIP-I-3F (5′-ATGAATTCCCGCCCGTCCAAATTC-3′) and vMIP-I-5R; vMIP-I-4F (5′-ATGAATTCCCAAAACCCGGAGTTATTTTGC-3′) and vMIP-I-5R; vMIP-II-1F (5′-CGGAATTCGTTATGGACACCAAGGGC-3′) and vMIP-II-5R (5′-GGCAGTCGACTCTTCAGCGAGCAGTGACTG-3′); vMIP-II-2F (5′-GGGAATTCCTGGGAGCGTCCTGGCATAGAC-3′) and vMIP-II-5R; vMIP-II-3F (5′- AAGAATTCTTACCACAGGTGCTTCTGTCC-3′) and vMIP-II-5R; and vMIP-II-4F (5′-TGGAATTCAAGCCGGGTGTGATATTTTTG-3′) and vMIP-II-5R. The PCR products were cloned into pCR2.1 (Invitrogen, Carlsbad, CA) and confirmed by sequencing. The products were digested with the *Eco*RI and *Sal*I restriction enzymes and were cloned into pGEX-5X-1 (GE Healthcare). The PCR conditions for all products were as follows: 25 cycles of 94 °C for 1 min, 55 °C for 1 min, and 72 °C for 2 min in a TP480 PCR thermal cycler (Takara Shuzo, Kyoto, Japan).

Immunization and generation of monoclonal Abs against vMIP-I and vMIP-II

In mice, anti-vMIP-I and -vMIP-II antibodies were raised against the GST-vMIP-I and GST-vMIP-II fusion protein, respectively. These GST fusion proteins were purified on a glutathione-Sepharose 4B column (GE Healthcare), and the GST-vMIP-I and the GST-vMIP-II fusion proteins were conjugated to keyhole limpet hemocyanin KLH (Calbiochem. Co., La Jolla, CA). Mice were initially immunized with 250 μg each of the purified GST-vMIP-I or -II fusion protein in Freund's complete adjuvant administered to the peritoneal cavity, and 200 μg of the antigen in Freund's incomplete adjuvant were injected again 14 and 28 days after the first injection. The mice were exsanguinated 7 days after the last injection. To generate MAbs against vMIP-I and vMIP-II, hybridomas were established by fusing splenocytes from the hyperimmune mice using a nonproducing myeloma cell line, Sp-2/0-Ag14 (ATCC, Manassas, VA). After selection in medium containing hypoxanthine-aminopterin-thymidine, cells secreting MAbs were screened by immunofluorescence assays (IFA). The TPA-induced and -uninduced BCBL-1 cells were fixed in acetone and exposed to supernatants of the hybrid cells. Clones secreting antibodies reactive with TPA-stimulated BCBL-1 cells were expanded and isolated by limiting dilutions.

Transfection analysis of vMIP-I and vMIP-II

To express the vMIP-I and vMIP-II proteins, 293/EBNA cells were transfected with pCAGGS-vMIP-I and -vMIP-II plasmids using TransIT-LT1 (Mirus Bio LLC, Madison, WI). The transfected cells were incubated for 48 h in DMEM supplemented with 10% FCS. The cells were harvested and lysed with lysis buffer (0.05 M Tris-HCl [pH 8.0], 0.15 M NaCl, 0.5% sodium deoxycholate, 1% Triton X-100, 0.1% sodium-dodecyl sulfate [SDS]). The cell lysate was fractionated by electrophoresis on 16% polyacrylamide gel as described below.

Antibodies and Western blotting

The expression of vMIP-I and vMIP-II in BC-3 cells stimulated with TPA was determined with MAbs against vMIP-I and vMIP-II, respectively, as noted above. The concentration of proteins extracted from BC-3 cells was normalized using a BCA Protein Assay Kit (Thermo Fisher Scientific Inc., Rockford, IL). The samples were subjected to SDS-15% polyacrylamide gel electrophoresis under reducing conditions, and were electrophoretically transferred to PVDF membranes (Bio-Rad Laboratories, Hercules, CA). The membranes were blocked for 1 h while being shaken at room temperature in PBS containing 0.05% Tween 20 and 5% w/v nonfat skim milk. The membranes were incubated with a primary antibody and were then incubated for 1 h with an appropriate dilution of horseradish peroxidase (HRP)-conjugated goat anti-mouse IgG antibodies (Santa Cruz Biotechnologies, Santa Cruz, CA). The primary antibody against actin, anti-actin (Ab-1) mouse MAb, was purchased from Merck (Merck KGaA, Darmstadt, Germany). The bound HRP-labeled antibodies were detected with a West Pico substrate kit for horseradish peroxidase (Thermo Fisher Scientific Inc).

IFA

BC-3 cells (10^7 cells) in RPMI 1640 medium with supplements were induced with 25 ng/ml TPA (Sigma Chemical Co., St. Louis, MO). The cells were collected after 0, 4, 8, 12, 24, 48, and 60 h for analysis of the expression kinetics, and for cellular localization analysis 48 h after exposure to TPA. The cells were washed in phosphate-buffered saline (PBS), pH 7.4, and spotted on glass slides. The spots were air-dried, then fixed in ice-cold acetone for 10 min. The cells were then washed with a washing buffer (PBS supplemented with 0.1% Triton X-100) for 15 min, and incubated with either an anti-vMIP-I or an anti-vMIP-II MAb (diluted 1:100 in IFA dilution buffer [PBS containing 2% bovine serum albumin, 0.2% Tween-20, and 0.05% NaN_3]) for 1 h at 37 °C. Then, the slides were washed with the washing buffer, and incubated for 1 h at room temperature with a pre-standardized diluted fluorescein isothiocyanate (FITC)-conjugated goat anti-mouse IgG (Tago Immunologicals, Camarillo, CA). The slides were washed and stained with 4′, 6′-diamidino-2-phenylindole (DAPI) to detect nuclei and were mounted with 50% (v/v) glycerol in PBS. For formalin-fixed paraffin-embedded tissues, antigen retrievals were performed on the de-paraffined sections using citrate buffer. Alexa 488 or 568-conjugated

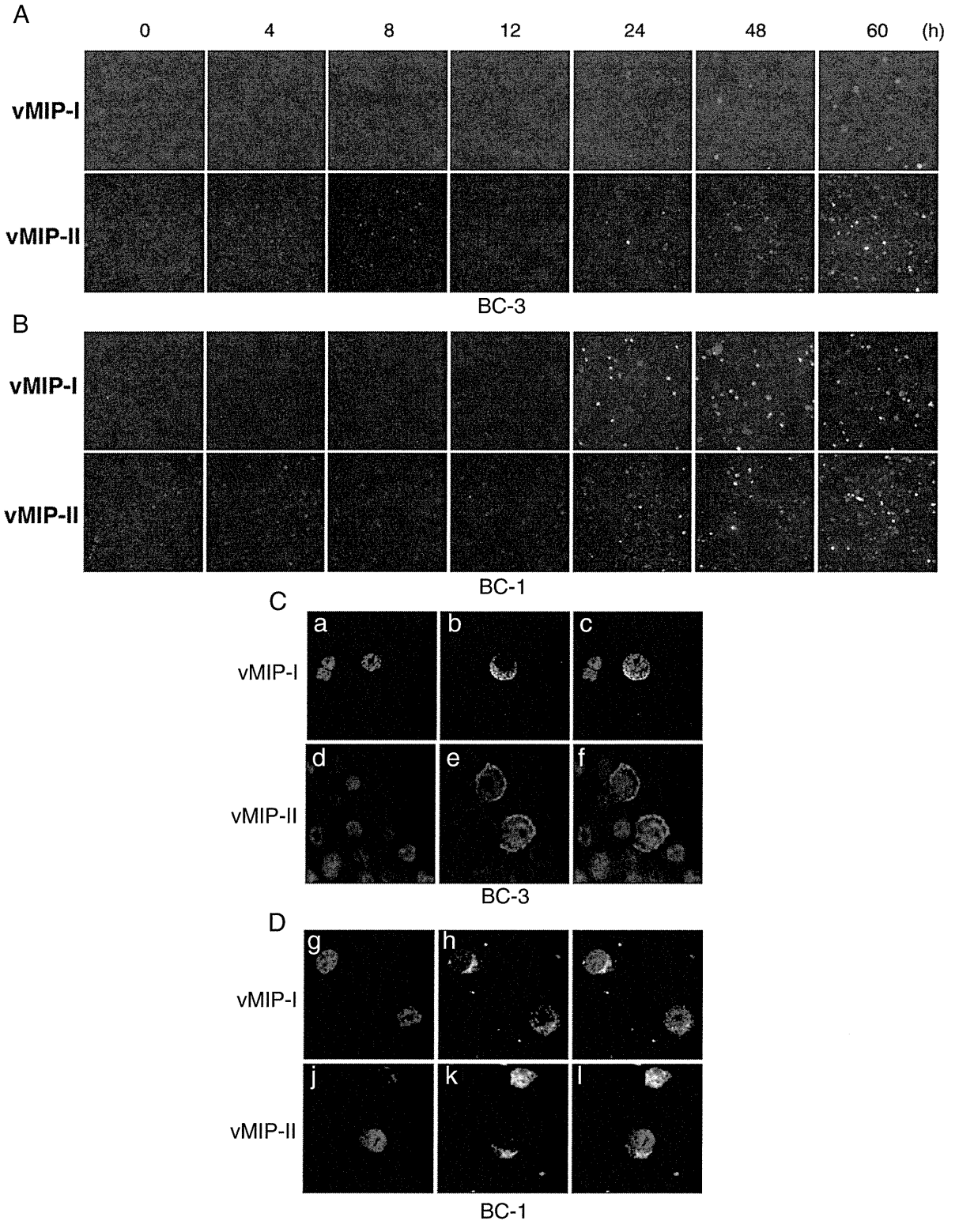

Fig. 4. Expression of vMIP-I and vMIP-II in BC-3 and BC-1 cells by IFA. After 4, 8, 12, 24, 48, and 60 h, BC-3 (A) and BC-1 (B) cells were labeled either with the anti-vMIP-I (upper) or the anti-vMIP-II (lower) MAb followed by goat anti-mouse FITC-conjugated Abs. FITC photomicrographs showing anti-vMIP-I and anti-vMIP-II immunoreactivity in BC-3 and BC-1 cells treated with TPA. (C) Cellular localization of vMIP-I and vMIP-II in BC-3 (C) and BC-1 (D) cells. The cells were stained with DAPI (a, d, g and j), and the localization of vMIP-I and vMIP-II was visualized by IFA with anti-vMIP-I or -vMIP-II MAbs (b, e, h and k); panel a and b, d and e, g and h, and j and k were merged (c, f, i and l). Fluorescence photomicrographs revealed anti-vMIP-I and -vMIP-II immunoreactivity using FITC-conjugated anti-mouse IgG MAb.

anti-mouse or rabbit antibodies (Invitrogen) were used as the secondary antibodies. Confocal microscopic analysis was performed (FV-1000, Olympus, Tokyo, Japan), and the contrast was adjusted before the images were exported as TIFF files to Adobe Photoshop.

Immunohistochemistry

Formalin-fixed paraffin-embedded tissues from KS and MCD patients, and those from an animal model of KSHV-associated solid lymphoma

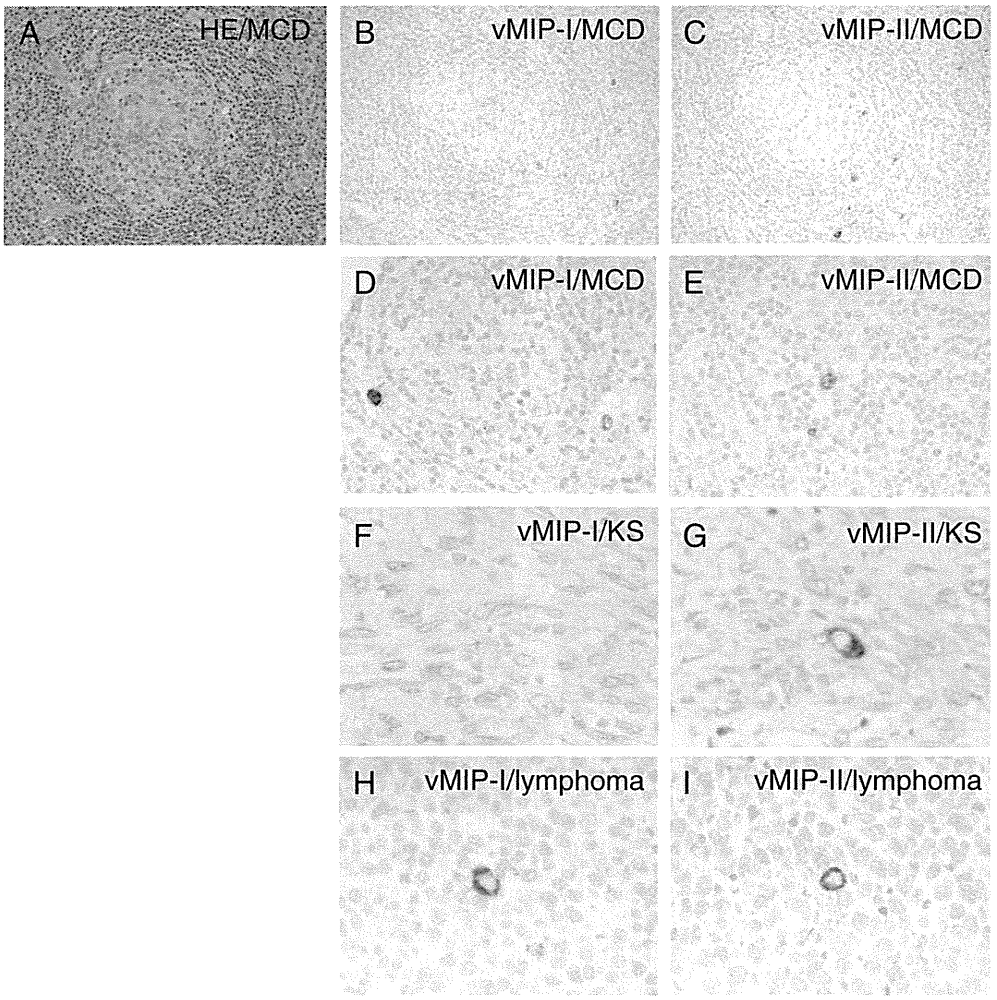

Fig. 5. Expression of vMIP proteins in KSHV-associated diseases. (A–C) Hematoxylin and eosin staining and immunohistochemistry for vMIPs in serial sections of a tissue sample from a patient with MCD. Brown stains indicate positive signals. The nucleus was counter-stained by hematoxylin. (D and E) Higher magnification view of vMIPs expression in an MCD case. Some large lymphocytes in the mantle zone were stained. (F and G) vMIP-I and vMIP-II expression in a KS sample. (H and I) Expression of vMIPs in an animal model of KSHV-associated lymphoma in SCID mice.

were sectioned and stained with hematoxylin and eosin (H&E). Immunohistochemistry of the serial sections was performed with either the anti-vMIP-I or -II MAb. For the second- and third- phase reagents used for immunostaining, a CSAII kit (DAKO, Copenhagen, Denmark) was used. An animal model of KSHV-associated solid lymphoma, which was established as described previously (Katano et al., 2000b), was also subjected to immunohistochemical analysis. Briefly, TY-1 cells were inoculated into the subcutaneous tissue of mice with severe combined immunodeficiency (SCID). One month after inoculation, lymphomas appeared in the subcutaneous region at the inoculation site. Lymphoma cells contained the KSHV genome, and expressed various viral proteins of KSHV (Katano et al., 2000b).

Table 1
Expression of vMIP-I and vMIP-II in MCD and KS tissue samples.

	KSHV proteins, (+)/total	
Cases	vMIP-I	vMIP-II
MCD	(3)/3	(3)/3
KS	(0)/5	(2)/8

Chemotaxis assays

Chemotaxis assays were performed as described previously (Nakano et al., 2003). Briefly, THP-1 cells were washed twice with chemotaxis buffer, 0.5% bovine serum albumin, 20 mM HEPES, pH 7.4, in RPMI 1640. Migration of cells was assessed in a cell culture chamber (Costar, Cambridge, MA), with the upper and lower compartments separated by a 3 μm pore size polycarbonate filter (???). The lower compartment of the chamber was filled with dilutions of vMIP-I, vMIP-II (R&D Systems, Minneapolis, MN) or with PBS alone, and/or with each 10 μg/ml anti-vMIP-I or -vMIP-II MAbs at a volume of 600 μl. The upper compartment contained 100 μl of THP-1 cell suspensions in chemotaxis buffer (10^5 cells/well). The chambers were then incubated for 4 hours at 37 °C, 5% CO_2, and spun at 300 x g, 4 °C, for 5 min. Finally, the cells from the lower compartment were counted.

Results

Specificity of the anti-vMIP-I MAb and the anti-vMIP-II MAb

In order to check specificity of the MAbs, we transfected vMIP-I and vMIP-II expression vectors (pCAGGS-vMIP-I, and -II) into 293/EBNA

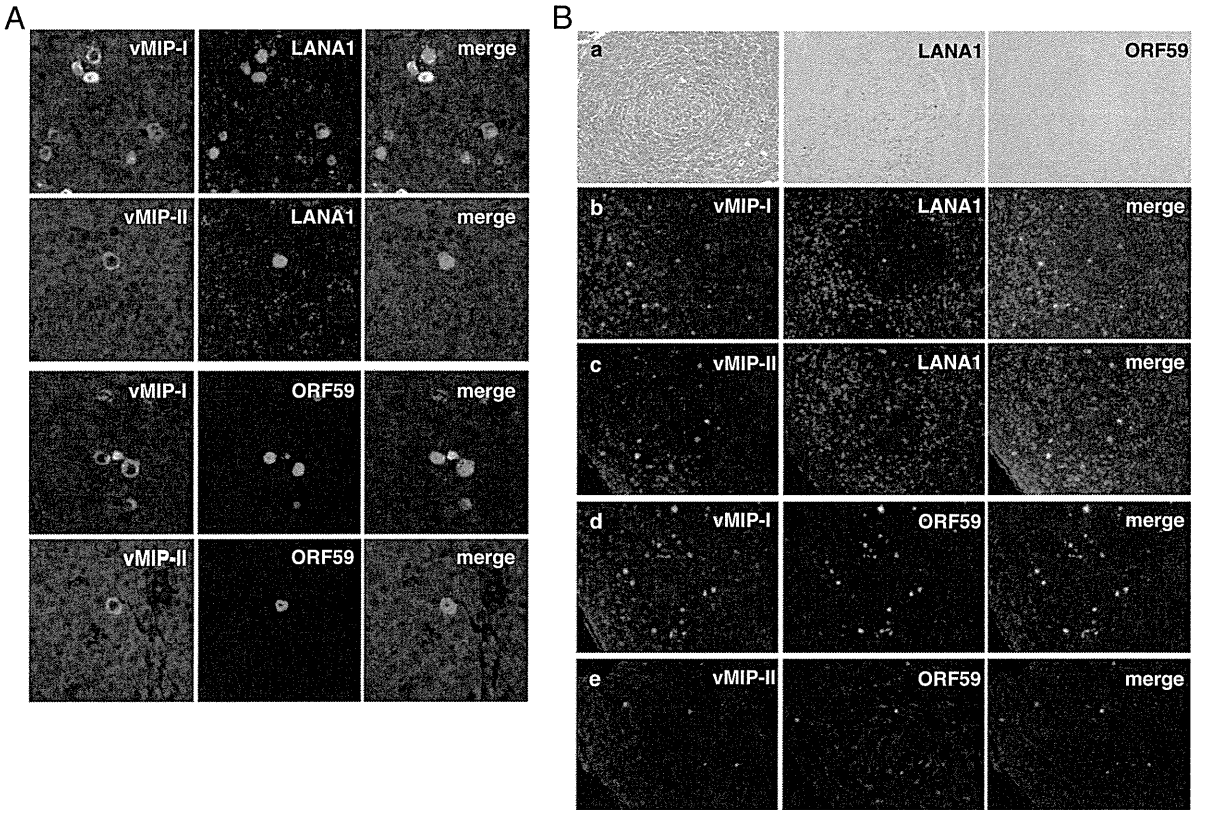

Fig. 6. (A) Expression of vMIPs. LANA1 and ORF59 in the animal model of KSHV-associated solid lymphoma by confocal microscopy. vMIPs were labeled with Alexa 488 (green). LANA1 (upper panels) and ORF59 (lower panels) were labeled with Alexa 568 (red). (B) Expression of vMIPs in MCD. (a) HE staining and immunohistochemistry of LANA1 and ORF59. (b–e) Immunofluorescence assay on MCD lesion. A germinal center is shown in the center of each panel. This case is KSHV-positive large B cell lymphoma arising in MCD.

cells, respectively. The total lysate of the transfected cells was subjected to Western blot analysis. vMIP-I and vMIP-II proteins were detected with anti-vMIP-I or vMIP-II MAbs, respectively (Fig. 1). These antibodies did not show cross-reactivity each other.

Epitope mapping of the anti-vMIP-I and anti-vMIP-II MAbs

We established hybridoma clones secreting MAbs against vMIP-I and vMIP-II, respectively. To map the regions of vMIP-I and vMIP-II where anti-vMIP-I and anti-vMIP-II antibody reacted, a series of GST-fused vMIP-I and vMIP-II deleted proteins were constructed as described in Fig. 2C and F, and used for Western blot analysis with an anti-GST antibody (Santa Cruz Biotechnology Inc), (Fig. 1A, D) and the anti-vMIP-I or the anti-vMIP-II (Fig. 1B, E) antibody, respectively. The results showed that all GST-vMIP-I and GST-vMIP-II fusion proteins interacted with the anti-GST antibody (Fig. 2A, D) and showed that GvM1-Full, GvM1-D1, and GvM1-D2 reacted with the anti-vMIP-I antibody, whereas GvM1-D3 did not (Fig. 1B), and GvM2-Full and GvM2-D1 reacted with the anti-vMIP-II antibody, whereas GvM2-D2, and GvM2-D3 did not (Fig. 2E). Thus, these results demonstrated that an anti-vMIP-I MAbs was successfully generated and suggest that the amino acid residues 61 to 95 of vMIP-I could be a major epitope reacted with the anti-vMIP-I antibody. On the other hand, the amino acid residues 24 to 42 of vMIP-II could be an epitope reacted with the anti-vMIP-II antibody.

Expression of vMIP-I and vMIP-II in the KSHV-infected PEL cell line

We tested vMIP-I and vMIP-II expression in KSHV and Epstein Barr virus (EBV) dually infected PEL cell lines (BC-1), KSHV infected PEL cell lines (BC-3) and in non-infected Burkitt's lymphoma cell line (BJAB), and detected them in TPA-stimulated BC-3 and BC-1 cells with developed antibodies, but not in BJAB cells non-stimulated BC-3 or BC-1 cells (Fig. 2A, B). In a KSHV infected PEL cells, BC-1 and BC-3, vMIP-I and vMIP-II were detected around at 10 kDa, which matches the size deduced from amino acids length (Fig. 3C, D). Actually, vMIP-I was detected from 6 hours post induction and vMIP-II was at 24 hours in BC-3 cells (Fig. 3C), and vMIP-I and vMIP-II were detected at 24 h in BC-1 cells (Fig. 3D). In the immunofluorescence microscopy, the number of vMIP-II expressing cells seemed to be more than that of vMIP-I in BC-3 cells (Fig. 4A, B). In order to analyze the cellular localization of vMIP-I and vMIP-II protein, BC-3 and BC-1 cells stimulated with TPA were doubly labeled with DAPI (Fig. 4C, a, d and D, g, j), and either the anti-vMIP-I MAb (Fig. 4C, b and D, h) or the anti-vMIP-II MAb (Fig. 4C, e and D, k). Merged images were shown in Fig. 4C, c, f, and D, i, l). The vMIP-I and the vMIP-II clearly showed cytoplasm and possibly membranes in TPA-induced BC-3 and BC-1 cells (Fig. 4C, b, e, and D, h, k).

Expression of vMIPs in KSHV-associated diseases

To know the expression of vMIPs in KSHV-associated diseases, immunohistochemistry for vMIPs was performed on pathological samples of eight KS cases, three MCD cases, and the animal model of KSHV-associated solid lymphoma (Fig. 5). Immunohistochemistry demonstrated that vMIP-I and vMIP-II were detected in some cells in the mantle zone of germinal center and the interfollicular zone in KSHV-positive MCD samples (Fig. 5A to E). Both vMIP-I and vMIP-II were detected predominantly in the cytoplasm of large lymphocytes. The numbers of positive cells varied among three MCD cases examined. On the other

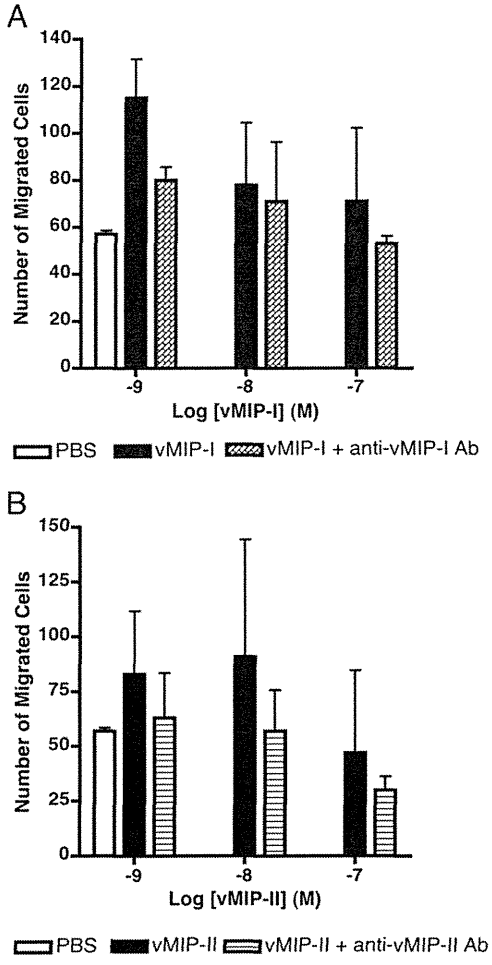

Fig. 7. Neutralizing activity of anti-vMIP-I and -vMIP-II MAbs. THP-1 cell migration in response to increased concentrations of vMIP-I and vMIP-II (1, 10, 100 nM), and the neutralizing activity of 10 μg/ml anti-vMIP-I and -vMIP-II MAbs against vMIP-I and vMIP-II were measured, as outlined in Materials and Methods, by using the transwell migration assay system. Various doses of vMIP-I and vMIP-II were tested for their ability to induce the chemotaxis of THP-1 cells. The data presented are from one experiment, and are representative of the triplicate experiments performed. The error bars indicate the standard deviations of three independent experiments.

hand, any positive signal of vMIP-I was not observed in all KS cases (Fig. 5F, G). vMIP-II was rarely detected in the cytoplasm of spindle cells in two KS cases at the nodular stage out of eight KS cases. In the samples of animal model of KSHV-associated solid lymphoma, both vMIP-I and vMIP-II were detected in the cytoplasm of a part of lymphoma cells (Fig. 5H, I). These data showed that vMIP-I and vMIP-II were expressed in cells in MCD and KSHV-associated lymphoma, but vMIP-II was rarely in KS (Table 1). To know the association of vMIPs expression with expression of other KSHV-encoded proteins, we examined immunofluorescence assay on KSHV-associated diseases. Since, all KSHV-infected cells express LANA1, vMIPs-positive cells were positive for LANA1. However, expression pattern of LANA1 showed diffuse nuclear staining in vMIPs-positive cells in the animal model of KSHV-associated solid lymphoma (Fig. 6A). Confocal microscopy revealed that vMIP-I stain showed usually cytoplasmic pattern, but rarely diffuse nuclear staining pattern *in vivo*. Almost all cells with vMIPs expression were also positive for ORF59 protein, a lytic protein of KSHV. IFA also demonstrated that vMIPs-positive cells expressed LANA1 at various levels in MCD clinical samples (Fig. 6B, a to c). A large portion of vMIPs-positive cells also expressed ORF59 protein in MCD (Fig. 6B, d, e). These data suggest that vMIPs are expressed by cells with KSHV-lytic infection in KSHV-associated MCD and lymphoma.

Neutralization of vMIP-I and vMIP-II by anti-vMIP-I and anti-vMIP-II MAbs

We examined whether the anti-vMIP-I and anti-vMIP-II MAbs could neutralize the chemoattractant of vMIP-I and vMIP-II to induce the migration of THP-1 cells. As expected, vMIP-I and vMIP-II induced migration of THP-1 cells (Fig. 7A, B), but not with PBS alone. However, anti-vMIP-I and anti-vMIP-II MAbs inhibited respective vMIP-I and vMIP-II-induced cell migration of THP-1 cells at 10 μg/ml final concentration.

Discussions

It was known that KSHV encodes three chemokine genes of the so-called viral macrophage inflammatory proteins: *vMIP-I*, *vMIP-II*, and *vMIP-III* in the genome. Analysis of the translated amino acid sequence indicate that the vMIP-I and vMIP-II gene have four conserved cysteines capable of forming two essential disulfide bonds (first cysteine and third cysteine, and second cysteine and fourth cysteine). The family of chemokines comprises CC, CXC, C, and CX_3C subfamilies. The vMIP-I and vMIP-II have four cysteines, the first two of which are found in the sequence of CC, which correspond to the CC profile. These gene products were expressed in the phase of KSHV lytic infection (Moore et al., 1996; Sun et al., 1999). Both vMIP-I and vMIP-II were expressed in a KSHV-infected cell lines, BC-3, which had been treated with TPA. Mono-specific polyclonal Abs against vMIP-I and vMIP-II have been described in previous studies that investigated the localization of vMIPs in PEL cells (Nakano et al., 2003). In the present study, we developed the respective MAbs that reacted either with KSHV vMIP-I or vMIP-II. We first applied these MAbs against KSHV vMIP-I and vMIP-II to detect KSHV-infected BC-3 and BC-1 cells by Western blotting and immunofluorescence assay. The Western blot analysis revealed that both the anti-vMIP-I and the anti-vMIP-II MAbs reacted to the 10-kDa proteins considered specific to the respective vMIP protein. The anti-vMIP-I MAb was shown to be reactive with the epitopes in the middle of the protein (sequence, PPVQILKEWYPTSPAC), and the epitope of the anti-vMIP-II MAb was shown to be reactive at the N-terminal end (sequence, LGASWHRPDKCCLGYQKRP). Further immunofluorescence analysis of the cellular localization of both vMIP-I and vMIP-II with anti-vMIP-I and anti-vMIP-II MAb showed a cytoplasmic pattern of expression in BC-3 and BC-1 cells. As the results indicated that these gene products were expressed in the cytoplasm, it might be located at the KSHV-infected BC-3 or BC-1 cells membrane prior to secretion. An investigation of the antigenic specificities of MAbs against KSHV vMIP-I and vMIP-II in MCD and KS patients has not yet been reported. Here, immunohistochemical analysis detected only vMIP-II in samples from both KS and MCD patients, but vMIP-I was not detected in KS cases: however, both vMIP-I and vMIP-II proteins were expressed in some cells in the interfollicular zone of MCD tissues. Lytic proteins of the KSHV such as K8, RTA, and ORF59 have been detected in large lymphocytes in the mantle zone of MCD cases (Dupin et al., 1999; Katano et al., 2000a). The expression of vMIPs showed a similar pattern to that of the lytic proteins in MCD tissues. In contrast, lytic protein expression, including that of vMIPs, was rare in the KS lesions (Abe et al., 2006). In the present study, we demonstrated that vMIPs were expressed in the cells expressing ORF59 protein. Thus, our data clearly indicated that the expression of vMIPs is associated with lytic infection in individual cells affected by KSHV-associated diseases. Human monocytic cell line THP-1 respond to various chemokines suggesting that they express receptors for these chemokines (Wang et al., 1993). Previous study, vMIP-I and vMIP-II were shown chemotaxis in THP-1 cells (Nakano et al., 2003). It has been reported that vMIP-I acts as a specific agonist for CC chemokine receptor 8 (CCR8) (Dairaghi et al., 1999; Endres et al., 1999) and vMIP-II shows a Ca^{2+} flux as a specific agonist for CCR3 (Boshoff et al., 1997). Our data showed anti-vMIP-I and anti-vMIP-II MAbs were able to neutralize vMIP-I- and vMIP-II-mediated chemotaxis in THP-1 cells. However, neutralizing activities

of anti-vMIP-I MAb was apparently low, even the addition of 10 μg/ml MAbs. These findings support the assumption that anti-vMIP-I and -vMIP-II MAbs-blocked chemotaxis in THP-1 cells act through binding to the certain amino acid residue of vMIP-I and vMIP-II.

In summary, MAbs developed specifically for this series were used to detect vMIP-I and vMIP-II in MCD and KS tissues, which may account for certain clinical features of MCD and KS. To gain a better understanding of these important viral genes, additional studies will be needed that focus on revealing vMIP-I and vMIP-II expression profiles during lytic infection. Taken together, these studies provide an insight into the pathogenesis of the contribution of vMIP-I and vMIP-II to the lytic induction of KSHV. These MAbs could serve as useful tools to clarify the pathogenesis of KSHV-related diseases.

Acknowledgments

This study was supported by a grant for Research on Publicly Essential Drugs and Medical Devices from the Japan Health Sciences Foundation (SAA4832), Health and Labor Sciences Research Grants (to HK, No. H23-AIDS-Ippan-002) from the Ministry of Health and by a grant from PRESTO of the Japan Science and Technology Corporation (200154023).

References

Abe, Y., Matsubara, D., Gatanaga, H., Oka, S., Kimura, S., Sasao, Y., Saitoh, K., Fujii, T., Sato, Y., Sata, T., Katano, H., 2006. Distinct expression of Kaposi's sarcoma-associated herpesvirus-encoded proteins in Kaposi's sarcoma and multicentric Castleman's disease. Pathol. Int. 56, 617–624.

Arvanitakis, L., Mesri, E.A., Nador, R.G., Said, J.W., Asch, A.S., Knowles, D.M., Cesarman, E., 1996. Establishment and characterization of a primary effusion (body cavity-based) lymphoma cell line (BC-3) harboring kaposi's sarcoma-associated herpesvirus (KSHV/HHV-8) in the absence of Epstein-Barr virus. Blood 88, 2648–2654.

Benelli, R., Barbero, A., Buffa, A., Aluigi, M.G., Masiello, L., Morbidelli, L., Ziche, M., Albini, A., Noonan, D., 2000. Distinct chemotactic and angiogenic activities of peptides derived from Kaposi's sarcoma virus encoded chemokines. Int. J. Oncol. 17, 75–81.

Boshoff, C., Endo, Y., Collins, P.D., Takeuchi, Y., Reeves, J.D., Schweickart, V.L., Siani, M.A., Sasaki, T., Williams, T.J., Gray, P.W., Moore, P.S., Chang, Y., Weiss, R.A., 1997. Angiogenic and HIV-inhibitory functions of KSHV-encoded chemokines. Science 278, 290–294.

Cesarman, E., Chang, Y., Moore, P.S., Said, J.W., Knowles, D.M., 1995. Kaposi's sarcoma-associated herpesvirus-like DNA sequences in AIDS-related body-cavity-based lymphomas. N. Engl. J. Med. 332, 1186–1191.

Chang, Y., Cesarman, E., Pessin, M.S., Lee, F., Culpepper, J., Knowles, D.M., Moore, P.S., 1994. Identification of herpesvirus-like DNA sequences in AIDS-associated Kaposi's sarcoma. Science 266, 1865–1869.

Chen, S., Bacon, K.B., Li, L., Garcia, G.E., Xia, Y., Lo, D., Thompson, D.A., Siani, M.A., Yamamoto, T., Harrison, J.K., Feng, L., 1998. In vivo inhibition of CC and CX3C chemokine-induced leukocyte infiltration and attenuation of glomerulonephritis in Wistar–Kyoto (WKY) rats by vMIP-II. J. Exp. Med. 188, 193–198.

Dairaghi, D.J., Fan, R.A., McMaster, B.E., Hanley, M.R., Schall, T.J., 1999. HHV8-encoded vMIP-I selectively engages chemokine receptor CCR8. Agonist and antagonist profiles of viral chemokines. Biol. Chem. 274, 21569–21574.

Dupin, N., Fisher, C., Kellam, P., Ariad, S., Tulliez, M., Franck, N., van Marck, E., Salmon, D., Gorin, I., Escande, J.P., Weiss, R.A., Alitalo, K., Boshoff, C., 1999. Distribution of human herpesvirus-8 latently infected cells in Kaposi's sarcoma, multicentric Castleman's disease, and primary effusion lymphoma. Proc. Natl. Acad. Sci. U. S. A. 96, 4546–4551.

Endres, M.J., Garlisi, C.G., Xiao, H., Shan, L., Hedrick, J.A., 1999. The Kaposi's sarcoma-related herpesvirus (KSHV)-encoded chemokine vMIP-I is a specific agonist for the CC chemokine receptor (CCR)8. J. Exp. Med. 189, 1993–1998.

Katano, H., Sato, Y., Kurata, T., Mori, S., Sata, T., 2000a. Expression and localization of human herpesvirus 8-encoded proteins in primary effusion lymphoma, Kaposi's sarcoma, and multicentric Castleman's disease. Virology 269, 335–344.

Katano, H., Suda, T., Morishita, Y., Yamamoto, K., Hoshino, Y., Nakamura, K., Tachikawa, N., Sata, T., Hamaguchi, H., Iwamoto, A., Mori, S., 2000b. Human herpesvirus 8-associated solid lymphomas that occur in AIDS patients take anaplastic large cell morphology. Mod. Pathol. 13, 77–85.

Kledal, T.N., Rosenkilde, M.M., Coulin, F., Simmons, G., Johnsen, A.H., Alouani, S., Power, C.A., Luttichau, H.R., Gerstoft, J., Clapham, P.R., Clark-Lewis, I., Wells, T.N., Schwartz, T.W., 1997. A broad-spectrum chemokine antagonist encoded by Kaposi's sarcoma-associated herpesvirus. Science 277, 1656–1659.

Miller, G., Heston, L., Grogan, E., Gradoville, L., Rigsby, M., Sun, R., Shedd, D., Kushnaryov, V.M., Grossberg, S., Chang, Y., 1997. Selective switch between latency and lytic replication of Kaposi's sarcoma herpesvirus and Epstein-Barr virus in dually infected body cavity lymphoma cells. J. Virol. 71, 314–324.

Moore, P.S., Boshoff, C., Weiss, R.A., Chang, Y., 1996. Molecular mimicry of human cytokine and cytokine response pathway genes by KSHV. Science 274, 1739–1744.

Nakano, K., Isegawa, Y., Zou, P., Tadagaki, K., Inagi, R., Yamanishi, K., 2003. Kaposi's sarcoma-associated herpesvirus (KSHV)-encoded vMIP-I and vMIP-II induce signal transduction and chemotaxis in monocytic cells. Arch. Virol. 148, 871–890.

Niwa, H., Yamamura, K., Miyazaki, J., 1991. Efficient selection for high-expression transfectants with a novel eukaryotic vector. Gene 108, 193–199.

Schalling, M., Ekman, M., Kaaya, E.E., Linde, A., Biberfeld, P., 1995. A role for a new herpes virus (KSHV) in different forms of Kaposi's sarcoma. Nat. Med. 1, 707–708.

Soulier, J., Grollet, L., Oksenhendler, E., Cacoub, P., Cazals-Hatem, D., Babinet, P., d'Agay, M.F., Clauvel, J.P., Raphael, M., Degos, L., et al., 1995. Kaposi's sarcoma-associated herpesvirus-like DNA sequences in multicentric Castleman's disease. Blood 86, 1276–1280.

Sun, R., Lin, S.F., Staskus, K., Gradoville, L., Grogan, E., Haase, A., Miller, G., 1999. Kinetics of Kaposi's sarcoma-associated herpesvirus gene expression. J. Virol. 73, 2232–2242.

Wang, J.M., McVicar, D.W., Oppenheim, J.J., Kelvin, D.J., 1993. Identification of RANTES receptor on human monocytic cells: competition of binding and desensitization by homologous chemotactic cytokines. J. Exp. Med. 177, 699–705.

frontiers in
MICROBIOLOGY

EDITORIAL
published: 11 July 2012
doi: 10.3389/fmicb.2012.00237

For the future studies of Kaposi's sarcoma-associated herpesvirus

Keiji Ueda*

Division of Virology, Department of Microbiology and Immunology, Osaka University Graduate School of Medicine, Osaka, Japan
** Correspondence: kueda@virus.med.osaka-u.ac.jp*

Edited by:
Akio Adachi, The University of Tokushima Graduate School, Japan

It is 18 years since Kaposi's sarcoma-associated virus (KSHV), also called human herpesvirus 8 (HHV-8), was found from Kaposis' sarcoma (KS) by Chang et al. (1994). More than 8, 000 reports have been published so far and we have learned many things from this virus. I would like to say it is about time to look back previous studies and to think what to study next on the virus, and planed a topic to think what to study next on the virus for future.

Herpesviruses have relatively big genomes and encode a 100 genes or so. Thus, the virion assembly/structure, gene expression regulation and attachment/entry are complicated and have known only an iceberg of them. Studying the details how the viruses run their life cycles and cause diseases in their processes will lead to exploring new therapeutic drugs/methods.

A viral life cycle starts from attachment on the susceptible cells and then, entry into the cells, followed by the viral gene expression, the genome replication, the particle assembly and finally the daughter viruses egress out of the cells. This process is skillfully built and all the viral genes are required for the process, though there are essential genes and non-essential ones. Viral pathogenesis could be established during this process by the interaction between viruses and host cells, and individual host systems such as immune system. In this topic, although I would like to cover all the processes, thankfully, 15 specialists in each field have contributed for this topic.

Polizzotto et al. (2012) described clinical manifestations of KSHV-associated diseases. So far, there were few reports on clinical manifestations of primary KHSV infection. In this term, KSHV inflammatory cytokine syndrome (KICS) is a new concept and we might have been looked over an important disease sign on KHSV infection. We will have to be more careful about what happens in primary KSHV infection than before.

Fukumoto et al. (2011) describe KSHV infection from a pathologist's points of view. Pathologic study is very important to know what happens in the lesions. Currently, we are able to know what is going on only in the KSHV associated lesions such as Kaposi's sarcoma, multicentric Castleman's disease and primary effusion lymphomas (PEL) of human samples suffered from KSHV infection, but once an infection model is established, chronological pathologic studies will provide a lot of information on how KSHV-associated diseases are formed.

Chakraborty et al. (2012) review the entry mechanism of KSHV into cells. In general, herpesviruses can infect various kinds of cells *in vitro* including non-human cell lines, but the infectivity to B lymphocyte originated cells is very inefficient. Their report will give us a hint why such phenomenon happens.

An immediate early gene, *RTA* (reactivation and transcription activator) is very important for the viral lytic replication induction and shows multifunctions. We still have not understood how the factor functions. Guito and Lukac (2012) and Tsai et al. (2012) review or report mechanistic regulation of this strong transactivator, respectively.

Jackson et al. (2012) describe ORF57, which is also an interesting and multifunctional protein. This is involved in post-translational processes of the viral gene expression as sumoylation and ubiquitination described by Campbell and Izumiya (2012) and Ashizawa et al. (2012) respectively. We had believed that K-bZIP, a homolog of Epstein-Barr virus Zta was a transactivator and origin recognition factor in the lytic replication. K-bZIP, however, has other important roles for KSHV lytic replication. In latency, metabolism of LANA (latency-associated nuclear antigen) could be critical for KSHV-induced tumor formation and/or its phenotype.

Viral particle assembly is virologically an exciting and interesting field. There have been few reports on this, Sathish et al. (2012) try to search this issue.

The detail replication mechanism of KSHV in both lytic and latent phase has been still unclear. In latency, the virus is supposed to utilize host replication machinery including pre-replication complexes (pre-RC) for the viral replication initiation in the presence of LANA. The viral factor, LANA, is an essential factor, but its necessity has not been elucidated well. LANA binds with LANA-biding sites (LBS) and recruits origin recognition complexes (ORCs) on the viral replication origin (ori-P), which cannot account for necessity of the GC-rich element followed by LBS. Ohsaki and Ueda (2012) will give us a hint about this question.

Viral immune evasion system is very tactic to maintain its latency in case of herpesviruses. The maintenance of latency is then critical for the virus to wait for reactivation to produce daughter viruses, whose transition may a step for the viral oncogenic process. Lee et al. (2012) summarize KSHV immune evasion strategy and make a comment on the future landscape.

Kaposi's sarcoma-associated virus mediated tumorigenesis including PEL and KS has been still unclear, though there are many reports on individual viral putative oncogenes. KSHV has not been reported to infect and immortalize and/or transform endothelial cells or peripheral blood mononuclear cells *in vitro*. And thus, we have not known how the viral genes with oncogenic potentials such as *vFLIP*, *vCYC*, *vGPCR* and so on in addition to *LANA* cooperate in the viral oncogenic process. DiMaio and Lagunoff (2012) address on this issue and look forward for this field.

MicroRNA is one of the hottest research fields even in KSHV. This kind of small RNA molecule seems to have profound effects on cellular processes and then viral activities but their details have not been elucidated totally. KSHV lytic and latent phases are regulated by viral but also cellular microRNAs. Two specialists; Liang et al. (2011) and Gottwein (2012) reveals the microRNA world of KSHV.

And finally, we have to think about treatment of KSHV-associated tumors such as KS, PEL and a lympho-proliferative disease, multicentric Castleman's disease. It should be very hard to treat these tumors in the immunodeficient setting. It will be desirable if KSHV specific strategy is designed, since these tumors are very tightly linked with KSHV infection. Dittmer et al. (2012) contribute for this theme and discuss about it.

ACKNOWLEDGMENT

I would like to thank all contributors, and hope that this topic will be useful for the future study of KSHV.

REFERENCES

Ashizawa, A., Higashi, C., Masuda, K., Ohga, R., Taira, T., and Fujimuro, M. (2012). The ubiquitin system and Kaposi's sarcoma-associated herpesvirus. *Front. Microbiol.* 3:66. doi: 10.3389/fmicb.2012.00066

Campbell, M., and Izumiya, Y. (2012). Post-translational modifications of Kaposi's sarcoma-associated herpesvirus regulatory proteins–SUMO and KSHV. *Front. Microbiol.* 3:31. doi: 10.3389/fmicb.2012.00031

Chakraborty, S., Veettil, M. V., and Chandran, B. (2012). Kaposi's sarcoma associated herpesvirus entry into target cells. *Front. Microbiol.* 3:6. doi: 10.3389/fmicb.2012.00006

Chang, Y., Cesarman, E., Pessin, M. S., Lee, F., Culpepper, J., Knowles, D. M., and Moore, P. S. (1994). Identification of herpesvirus-like DNA sequences in AIDS-associated Kaposi's sarcoma. *Science* 266, 1865–1869.

DiMaio, T. A., and Lagunoff, M. (2012). KSHV induction of angiogenic and lymphangiogenic phenotypes. *Front. Microbiol.* 3:102. doi: 10.3389/fmicb.2012.00102

Dittmer, D. P., Richards, K. L., and Damania, B. (2012). Treatment of kaposi sarcoma-associated herpesvirus-associated cancers. *Front. Microbiol.* 3:141. doi: 10.3389/fmicb.2012.00141

Fukumoto, H., Kanno, T., Hasegawa, H., and Katano, H. (2011). Pathology of Kaposi's sarcoma-associated herpesvirus infection. *Front. Microbiol.* 2:175. doi: 10.3389/fmicb.2011.00175

Gottwein, E. (2012). Kaposi's sarcoma-associated herpesvirus microRNAs. *Front. Microbiol.* 3:165. doi: 10.3389/fmicb.2012.00165

Guito, J., and Lukac, D. M. (2012). KSHV Rta promoter specification and viral reactivation. *Front. Microbiol.* 3:30. doi: 10.3389/fmicb.2012.00030

Jackson, B. R., Noerenberg, M., and Whitehouse, A. (2012). The Kaposi's sarcoma-associated herpesvirus ORF57 protein and its multiple roles in mRNA biogenesis. *Front. Microbiol.* 3:59. doi: 10.3389/fmicb.2012.00059

Lee, H. R., Brulois, K., Wong, L., and Jung, J. U. (2012). Modulation of immune system by Kaposi's sarcoma-associated herpesvirus: lessons from viral evasion strategies. *Front. Microbiol.* 3:44. doi: 10.3389/fmicb.2012.00044

Liang, D., Lin, X., and Lan, K. (2011). Looking at Kaposi's sarcoma-associated herpesvirus-host interactions from a microRNA viewpoint. *Front. Microbiol.* 2:271. doi: 10.3389/fmicb.2011.00271

Ohsaki, E., and Ueda, K. (2012). Kaposi's sarcoma-associated herpesvirus genome replication, partitioning, and maintenance in latency. *Front. Microbiol.* 3:7. doi: 10.3389/fmicb.2012.00007

Polizzotto, M. N., Uldrick, T. S., Hu, D., and Yarchoan, R. (2012). Clinical manifestations of Kaposi sarcoma herpesvirus lytic activation: multicentric castleman disease (KSHV-MCD) and the KSHV inflammatory cytokine syndrome. *Front. Microbiol.* 3:73. doi: 10.3389/fmicb.2012.00073

Sathish, N., Wang, X., and Yuan, Y. (2012). Tegument proteins of Kaposi's sarcoma-associated herpesvirus and related gamma-herpesviruses. *Front. Microbiol.* 3:98. doi: 10.3389/fmicb.2012.00098

Tsai, W. H., Wang, P. W., Lin, S. Y., Wu, I. L., Ko, Y. C., Chen, Y. L., Li, M., and Lin, S. F. (2012). Ser-634 and Ser-636 of Kaposi's sarcoma-associated herpesvirus RTA are involved in transactivation and are potential Cdk9 phosphorylation sites. *Front. Microbiol.* 3:60. doi: 10.3389/fmicb.2012.00060

Received: 04 June 2012; accepted: 15 June 2012; published online: 11 July 2012.
Citation: Ueda K (2012) For the future studies of Kaposi's sarcoma-associated herpesvirus. Front. Microbio. 3:237. doi: 10.3389/fmicb.2012.00237
This article was submitted to Frontiers in Virology, a specialty of Frontiers in Microbiology.

Blood & Lymph

Ueda, J Blood Lymph 2012, 2:3
http://dx.doi.org/10.4172/2165-7831.1000e109

Editorial Open Access

Kaposi's Sarcoma-Associated Herpesvirus Induced Tumorigenesis; How Viral Oncogenic Insults are Evaded

Keiji Ueda*

Division of Virology, Department of Microbiology and Immunology, Osaka University Graduate School of Medicine, Japan

Some viral infections in human are strongly related to cancer formation. Apart from retrovirus induced cancer formation seen in rodents and avian, virus induced cancer formation in human seems to be very complicated. In human, mainly DNA viruses such as papillomavirus, hepatitis B virus (HBV), Epstien-Barr virus (EBV), and Kaposi's sarcoma-associated herpes virus (KSHV) are etiological agents and some RNA viruses such human T-cell leukemia virus and hepatitis C virus (HCV) are involved in their specific cancer formation. It takes long time for the viruses to cause cancers and we do not have good systems to observe how the viral infection leads to cancer formation.

KSHV is belonging to gamma-herpesviridae and an agent involved in the formation of Kaposi's sarcoma (KS), primary effusion lymphoma (PEL) and multicentric Castelman's disease (MCD).

The virus infection has a very strong link with these cancers. The mechanism how the virus causes such cancers is, however, still enigmatic and remains to be elucidated. KSHV latent infection should be important in terms that this type of infection provides with an origin of the related cancers. But, many genes with oncogenic activity of this virus are lytic genes, which are expressed only in the lytic phase.

As mentioned above, virus induced carcinogenesis is very complicated and is attractive to take an insight how the virus causes related cancers [1].

KSHV expresses an extremely limited number of viral genes such as latency-associated nuclear antigen (LANA), viral cyclin (v-cyc), viral FLICE inhibitory protein (vFLIP), kaposin and viral interferon regulatory factor-3 (vIRF-3) and 17 viral microRNAs in latency. The genes build an active gene locus in the KSHV genome in latency.

Among them, v-CYC, a homolog of cellular D-type cyclins, functions as an oncogene to deregulate cellular proliferation which leads to DNA damage response (DDR) and p53 induced apoptosis. Normal cells respond to oncogenic insults and cannot be easily transformed by choosing suicide pathway through p53 [2]. If the virus survives this situation, there must be a mechanism and this is one of ways how KSHV causes cancers.

In this point a recent report from Leidal et al. [1] is attractive for an insight to link the v-CYC induced oncogenic insult with subversion of this activity by vFLIP and how the virus causes related cancers. They found that v-CYC caused autophagy induced senescence and/or apoptosis. On the other hand, vFLIP is known for an autophagy inhibitor as well as an NF-kB activator [3,4]. And thus, vFLIP functions to evade from v-CYC induced oncogenic insult/senescence and make a direction of KSHV induced carcinogenesis.

However, we should be careful whether such a pathway happens in the natural infection course, since this kind of experiment is usually performed in over-expression system. Actually, vFLIP expression at the protein level has not been confirmed even in KSHV infected PEL cell lines and thus it is unclear whether such vFLIP activity is seen in the native situation.

In summary, a report from Liang seems to be very important to explain how KSHV causes cancers by connecting oncogene (v-CYC in this case) induced apoptosis and/or senescence [5]. Although there is no related report about the other human virus induced carcinogenesis, similar mechanisms might be stealthing.

References

1. Leidal AM, Cyr DP, Hill RJ, Lee PW, McCormick C (2012) Subversion of autophagy by Kaposi's sarcoma-associated herpesvirus impairs oncogene-induced senescence. Cell Host Microbe. 11: 167-180.
2. Lee JS, Li Q, Lee JY, Lee SH, Jeong JH, et al. (2009) FLIP-mediated autophagy regulation in cell death control. Nat Cell Biol 11: 1355-1362.
3. Levine B, Kroemer G (2008) Autophagy in the pathogenesis of disease. Cell 132: 27-42.
4. Ganem D (2010) KSHV and the pathogenesis of Kaposi sarcoma: listening to human biology and medicine. J Clin Invest 120: 939-949.
5. Liang C (2012) Viral FLIPping autophagy for longevity. Cell Host Microbe 11: 101-103.

***Corresponding author:** Keiji Ueda, Division of Virology, Department of Microbiology and Immunology, Osaka University Graduate School of Medicine, Japan, E-mail: kueda@virus.med.osaka-u.ac.jp

Received August 28, 2012; **Accepted** August 28, 2012; **Published** August 30, 2012

Citation: Ueda K (2012) Kaposi's Sarcoma-Associated Herpesvirus Induced Tumorigenesis; How Viral Oncogenic Insults are Evaded. J Blood Lymph 2:e109. doi:10.4172/2165-7831.1000e109

Neuroscience Research 73 (2012) 115–121

Contents lists available at SciVerse ScienceDirect

Neuroscience Research

journal homepage: www.elsevier.com/locate/neures

Overexpression of HGF attenuates the degeneration of Purkinje cells and Bergmann glia in a knockin mouse model of spinocerebellar ataxia type 7

Satsuki Noma[a,b], Wakana Ohya-Shimada[a], Masaaki Kanai[a], Keiji Ueda[b], Toshikazu Nakamura[c], Hiroshi Funakoshi[a,*]

[a] Center for Advanced Research and Education, Asahikawa Medical University, Asahikawa 078-8510, Japan
[b] Division of Virology, Department of Immunology and Microbiology, Osaka University Graduate School of Medicine, Osaka 565-0871, Japan
[c] Kringle Pharma Joint Research Division for Regenerative Drug Discovery, Center for Advanced Science and Innovation, Osaka University, Osaka 565-0871, Japan

ARTICLE INFO

Article history:
Received 28 February 2012
Received in revised form 6 March 2012
Accepted 6 March 2012
Available online 15 March 2012

Keywords:
Hepatocyte growth factor
c-Met
Polyglutamine disease
Glutamate transporter
GLAST
GLT-1
SCA

ABSTRACT

Spinocerebellar ataxia type 7 (SCA7) is an autosomal dominant disorder associated with cerebellar neurodegeneration caused by expansion of a CAG repeat in the ataxin-7 gene. Hepatocyte growth factor (HGF), a pleiotrophic growth factor, displays highly potent neurotrophic activities on cerebellar neurons. A mutant c-met/HGF receptor knockin mouse model has revealed a role for HGF in the postnatal development of the cerebellum. The present study was designed to elucidate the effect of HGF on cerebellar neurodegeneration in a knockin mouse model of SCA7 (SCA7-KI mouse). SCA7-KI mice were crossed with transgenic mice overexpressing HGF (HGF-Tg mice) to produce SCA7-KI/HGF-Tg mice that were used to examine the phenotypic differences following HGF overexpression. The Purkinje cellular degeneration is thought to occur *via* cell-autonomous and non-cell autonomous mechanisms mediated by a reduction of glutamate transporter levels in Bergmann glia. The Purkinje cellular degeneration and reduced expression of glutamate transporters in the cerebellum of SCA7-KI mice were largely attenuated in the SCA7-KI/HGF-Tg mice. Moreover, phenotypic impairments exhibited by SCA7-KI mice during rotarod tests were alleviated in SCA7-KI/HGF-Tg mice. The bifunctional nature of HGF on both Purkinje cells and Bergmann glia highlight the potential therapeutic utility of this molecule for the treatment of SCA7 and related disorders.

1. Introduction

Spinocerebellar ataxia type 7 (SCA7) is a progressive inherited disorder characterized by ataxia and neurodegeneration of the cerebellum and retina (Ieraci et al., 2002). The disease is the result of an abnormal CAG repeat expansion in the ataxin-7 gene. SCA7 patients display ataxia in addition to neurodegeneration and neuronal death of Purkinje cells (Ieraci et al., 2002). SCA7 knockin mice also show a neurodegeneration of Purkinje cells (Yoo et al., 2003). Therefore, it is thought that the protection of Purkinje cells may represent a therapeutic strategy to combat SCA7.

Additionally, following findings suggest that Bergmann glial cells have been considered as another therapeutic target of the disease. Bergmann glia are cerebellum-specific astrocytes that are located around synapses between Purkinje cells and cerebellar granule cells or climbing fibers. The glial cells play a role in removing excess glutamate from synapses *via* two primary glutamate transporters, glutamate/aspartate transporter (GLAST) and glutamate transporter-1 (GLT-1) (Huang and Bordey, 2004). A mouse model that expresses expanded ataxin-7 specifically in Bergmann glia displays a neurodegeneration of Purkinje cells, indicating that a dysfunction of Bergmann glia contributes to the degeneration of Purkinje cells in SCA7 mice and thereby progression of the disease in a non-cell autonomous manner (Custer et al., 2006). Therefore, prevention of cell degeneration and concomitant increase of glutamate transporter function may represent a valid therapeutic strategy for SCA7.

Hepatocyte growth factor (HGF), which was first identified as a potent mitogen for mature hepatocytes (Nakamura et al., 1984, 1989), exhibits neurotrophic activities in a wide variety of neurons in the hippocampus, the cerebral cortex, the cerebellum, the brainstem (midbrain dopaminergic neurons) and the spinal cord (sensory and motor neurons) (Funakoshi and Nakamura, 2011). Recent experiments have indicated that HGF exerts neuroprotective effects on various neurons in animal models of cerebral ischemia, amyotrophic lateral sclerosis (ALS) and spinal cord injury (Funakoshi and Nakamura, 2011; Sun et al., 2002; Ishigaki et al., 2007; Kitamura et al., 2011; Miyazawa et al., 1998). In the cerebellum, HGF is expressed in Purkinje cells and granular cells, and plays a role in the cerebellum during both developmental and adult

* Corresponding author. Tel.: +81 166 68 2886.
E-mail address: hfuna@asahikawa-med.ac.jp (H. Funakoshi).

0168-0102/$ – see front matter © 2012 Elsevier Ireland Ltd and the Japan Neuroscience Society. All rights reserved.
doi:10.1016/j.neures.2012.03.001

stages (Honda et al., 1995; Ieraci et al., 2002). In a mutant with a partial loss of Met function, the cerebellum was smaller than in controls and showed abnormal foliation (Ieraci et al., 2002). In addition to the cell growth and development, HGF exhibits neuroprotective effects for mature granule cells in primary cerebellar neuron culture (Zhang et al., 2000; Hossain et al., 2002). Moreover, overexpression of HGF not only attenuates the degeneration of motor neurons as a neurotrophic factor but also maintains adequate levels of the astrocytic glutamate transporter GLT-1 in a transgenic mouse model of ALS (Sun et al., 2002). This evidence led us to hypothesize that HGF may have a therapeutic potential on cerebellar neurons and Bergmann glia, cerebellar astrocyte subpopulations, in a valid mouse model of SCA7 in which a targeted 266 CAG repeat segment (a length known to cause infantile disease onset) of ataxin-7 is knocked into the mouse *ATXN7/Sca7* locus. These mice show features, which resemble those observed in an infantile SCA7 patient (Yoo et al., 2003).

The purpose of this study was to examine the effect of HGF on the Purkinje cells and Bergman glia of SCA7-KI mice. For this purpose, transgenic mice overexpressing HGF in a neuron-specific manner (HGF-Tg mice; Sun et al., 2002) were crossed with SCA7 knockin mice (SCA7-KI mice; Yoo et al., 2003) and phenotypic comparisons were made in wild-type (WT), HGF-Tg, SCA7-KI, and SCA7-KI/HGF-Tg mice. Overexpression of HGF attenuated the shrinkage of Purkinje cells and prevented reduction of glutamate transporters in Bergmann glia and improved motor performance during the rotarod test in SCA7-KI mice.

2. Materials and methods

2.1. Animals

The SCA7 knockin ($Sca7^{266Q/5Q}$: SCA7-KI) mouse is a knockin mouse, which is a valid model of SCA7 that contains a targeted insertion of 266 CAG repeats (a number that causes infantile-onset disease) into the mouse *Sca7* locus. The mice were generously provided by Dr. Huda Zoghbi from the Baylor College of Medicine, Houston, TX (Yoo et al., 2003). Neuron-specific enolase (NSE)-promoter driven HGF transgenic (HGF-Tg) mice were generated and maintained as previously described (Sun et al., 2002). Heterozygous SCA7-KI male mice were crossed with heterozygous HGF-Tg female mice, which had been backcrossed with C57BL/6J mice for more than seven generations, to generate WT, heterozygous HGF-Tg, heterozygous SCA7-KI, and heterozygous SCA7-KI/HGF-Tg mice. Mouse genotypes were determined by dot blot hybridization or by polymerase chain reaction (PCR) using forward (5′-TTGTAGGAGCGGAAAGAATGTC-3′) and reverse (5′-CCACCCACAGATTCCACGAC-3′) primers for SCA7-KI and with forward (5′-CCAAACATCCGAGTTGGTTACT-3′) and reverse (5′-ATTACAACTTGTATGTCAAAAT-3′) primers for HGF-Tg mice. Experimental protocols were approved by the Animal Experimentation Ethics Committee of Asahikawa Medical University and Osaka University Graduate School of Medicine. All efforts were made to minimize animal discomfort and the number of animals used.

2.2. Cerebellar neuronal culture

Sixteen-day-old mouse embryos (E16) were obtained from timed pregnant C57BL/6J females (Japan SLC, Hamamatsu, Japan) that had been deeply anesthetized with isoflurane and euthanized *via* decapitation. Routinely, two pregnant females were processed in parallel. Immediately after euthanasia, uteri containing the embryos were removed and transferred into a sterile 100 mm tissue culture dish that was kept on ice and filled with ~20 ml ice-cold Leibovitz's L-15 medium. The cerebella were dissected using a stereomicroscope. After removing the meninges, the isolated cerebellar primordia were minced and transferred to a 15-ml Falcon tube containing L-15 medium. The supernatant was replaced with a pre-warmed 0.25% trypsin solution and the cerebella were incubated for 4–5 min at 37 °C with gentle shaking. Incubation was terminated by the addition of fetal bovine serum (JRH Biosciences, Brooklyn, Australia). Following the addition of DNase I and centrifugation, cells were dissociated by repeated pipetting and separated from non-dissociated tissue by sedimentation. The cells were seeded in plates precoated with poly-L-ornithine (500 μg/ml) at 2.5×10^5 cells/cm^2. Cultures were grown in neurobasal medium (Gibco Invitrogen, Grand Island, NY) supplemented with B27 (Gibco Invitrogen), 2 mM GlutaMaxI (Gibco Invitrogen), 1 mM adenine, 3 mM KCl, 1% heat-inactivated horse serum (Gibco Invitrogen), and a mixture of penicillin–streptomycin (100 U/ml and 100 μg/ml; Nacalai Tesque, Kyoto, Japan). From 2 days after seeding, 10 μM triiodothyronine (T3) and 1 μM Ara-C were added in order to mature Purkinje cells and to prevent the proliferation of non-neuronal cells. Half of the medium was replaced with fresh medium every 2 days. The cultures were maintained at 37 °C in a humidified incubator with 5% CO_2 and 95% air. The cells cultured for 14 days were washed with phosphate buffered saline (PBS) and fixed with 10% formalin in PBS.

2.3. Tissue preparation

Animals (WT, HGF-Tg, SCA7-KI, and SCA7-KI/HGF-Tg mice) at 10 weeks of age ($n = 3$ each) were deeply anesthetized with sodium pentobarbital and transcardially perfused with ice-cold PBS followed by ice-cold 4% paraformaldehyde in PBS. The cerebella were excised and immersed in the same fixative for several hours at 4 °C. Fixed tissues were immersed in 10% sucrose in PBS overnight at 4 °C, followed by 20% sucrose in PBS for 6 h at 4 °C, after which they were subsequently frozen in powdered dry ice or CO_2 gas. Frozen tissues were cut into either 16-μm or 40-μm thick sagittal sections using a Leica CM3050 S or CM1900 cryostat (Leica Microsystems GmbH, Wetziar, Germany).

2.4. Immunocytochemistry and immunohistochemistry

Formalin-fixed cerebellar neurons or cryosections were incubated in blocking buffer consisting of 10% normal goat serum (S26-100 mL, CHEMICON, Temecula, CA) and 0.3% Triton X-100 in PBS for an hour at room temperature followed by one or two of the following primary antibodies for 20 h at 4 °C: (1) mouse monoclonal anti-calbindin D28K antibody (1:250; 300, Swant, Marly, Switzerland); (2) mouse monoclonal anti-GFAP (glial fibrillary acidic protein) antibody (1:250; MAB3402, CHEMICON); (3) rabbit polyclonal anti-GFAP antibody (1:10; N150687, DAKO, Glostrup. Denmark); (4) rabbit polyclonal anti-c-Met antibody (1:50; SP260, Santa Cruz Biotechnology, Santa Cruz, CA); (5) rabbit polyclonal anti-rat HGF antibody (Ohya et al., 2007; Yamada et al., 1995) (6) guinea-pig polyclonal anti-GLAST antibody (1:500; AB1782, CHEMICON); (7) guinea-pig polyclonal anti-GLT-1 antibody (1:600; AB1783, CHEMICON). For immunostaining of phospho-c-Met, sections were incubated with Blocking One Histo (Nacalai Tesque) for an hour at room temperature, and then immunoreacted with rabbit polyclonal anti-phosphorylated c-Met antibody (1:200; C7240, Sigma, St. Louis, MO) in Signal Enhancer HIKARI B Solution (Nakalai Tesque) for 20 h at 4 °C. After washing the sections with PBS, immunoreactivity was visualized by incubating them further for 20 min at room temperature with secondary antibodies conjugated with Alexa Fluor 488, Alexa Fluor 546 or Alexa Fluor 647 diluted 1:600 (Invitrogen, Carlsbad, CA). Fluorescence-immunostained sections were observed under an Olympus FV1000

microscope (Olympus, Tokyo, Japan) or an All-in-One BZ-9000 Fluorescence microscope (KEYENCE, Osaka, Japan). Digital image Z-stacks were created, and projections were made from them using an Olympus FV1000 microscope and FV10-ASW software (Olympus). Fluorescence intensity was measured using the NIH Image J Program.

2.5. Quantification of cellular Purkinje cell size

Sixteen-micrometer stacks of cerebellar optical sections were collected using an All-in-One BZ-9000 Fluorescence microscope and Z-stack images were joined into sagittal images using BZ-II software (KEYENCE). These data were transferred into Neurolucida software (MBF Bioscience, Japan, Inc., Chiba, Japan). Four stacks (each 0.09 μm^2 in area) for each of three sections from WT, HGF-Tg, SCA7-KI, and SCA7-KI/HGF-Tg mice ($n=3$ each) were used to measure the cell sizes of calbindin-positive Purkinje cells. Quantification of cell size was performed as previously described with slight modifications (Yoo et al., 2003). Briefly, each cell surface was outlined manually. The perikaryon area of each cell was estimated to be the approximately circular area enclosed by the cell perimeter and the extension of the cell perimeter toward the initial point of dendrite extension. Partial cells and binary cell images were excluded based upon cell shape and relative fluorescence intensity.

2.6. Enzyme-linked immunosorbent assay (ELISA)

After the mice were placed under deep anesthesia with an overdose of sodium pentobarbital, the cerebella of WT, HGF-Tg, SCA7-KI, and SCA7-KI/HGF-Tg mice ($n=4$ each) were collected, quickly frozen and stored at −80 °C until used. Frozen tissue samples were homogenized, subsequently sonicated using a Bioruptor UCD-250 (Cosmo Bio Co., Ltd., Tokyo, Japan), and centrifuged at 4 °C. The supernatants were then used to quantify HGF protein levels using ELISA (Institute of Immunology Co., Ltd., Tokyo, Japan) as previously described (Kadoyama et al., 2007; Sun et al., 2002; Yamada et al., 1995).

2.7. Assessment of motor performance

A rotarod apparatus (Bioseb, Paris, France) was used to assess the ability of an animal to balance on an elevating rotating metal rod (Carter et al., 2001). Rotarod tests are a common tool of studies of mouse models of spinocerebellar ataxia (Yoo et al., 2003; Custer et al., 2006). In this study, 10-week-old mice (WT; $n=13$, HGF-Tg; $n=12$, SCA7-KI; $n=12$, SCA7-KI/HGF-Tg; $n=8$) were placed on the rotarod, the speed of which was set at 5 rpm initially and accelerated until reaching a speed of 20 rpm for 5 min. After taking a rest for more than 5 min, the latency to fall from the rotarod was measured for 5 min using the machine mode (initial rate of 5 rpm; acceleration until reaching 40 rpm for 10 min). The average latency to fall for each genotype was calculated.

2.8. Statistical analyses

Statistical analyses were carried out using StatView software version 5.0.1 (SAS institute, Cary, NC). Differences in the total intensities of immunostaining for HGF, GLAST, GLT1, size of Purkinje cells, and regional HGF levels in the cerebellum among the above animal models were all determined by one-way ANOVA with Fisher's PLSD tests. Latency to fall in rotarod tests was analyzed using the Student's t-test. The results are presented as the mean ± S.E.M. A value of $P<0.05$ was considered statistically significant.

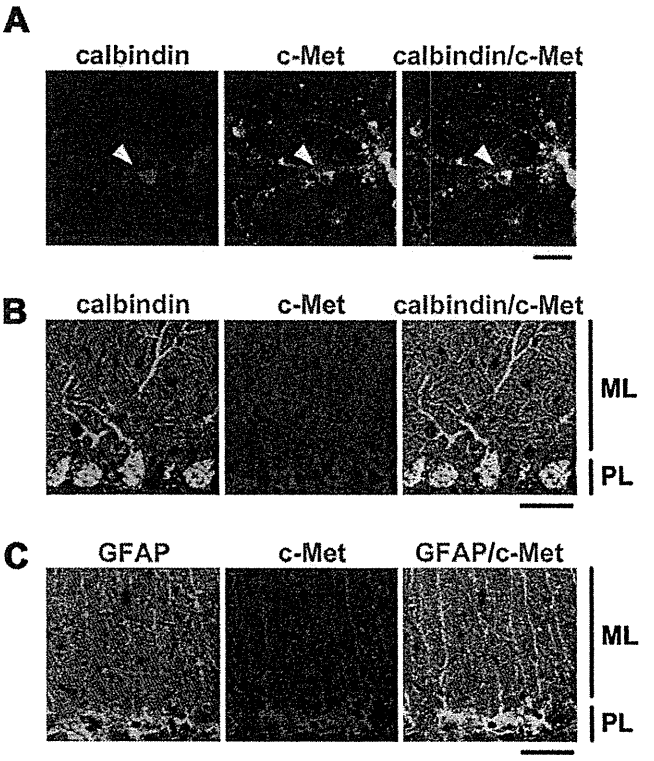

Fig. 1. Immunocytochemical and immunohistochemical localization of c-Met in cerebellar cells *in vitro* and *in vivo*. HGF receptor (c-Met) is expressed in Purkinje cells of the mouse cerebellum *in vitro* and *in vivo*. (A) Immunocytochemistry in primary neuronal cultures of the cerebellum from E16 mouse embryos. Purkinje cells show double immunoreactivity (white arrowheads) for calbindin (red) and c-Met (green) in culture. Bar, 30 μm. (B and C) Immunohistochemistry in 10-week-old wild-type (WT) mice. (B) Purkinje cells show double immunoreactivity against calbindin (green) and c-Met (red). PL, Purkinje cell layer; ML, molecular layer. Bar, 30 μm. (C) Bergmann glia show double immunoreactivity against GFAP (green) and c-Met (red). Bar, 30 μm. (For interpretation of the references to color in this figure caption, the reader is referred to the web version of the article.)

3. Results

3.1. c-Met is expressed in the cerebellar Purkinje cells in vitro

To assess whether cerebellar Purkinje cells are potential target cells of HGF, we first performed double immunostaining of c-Met (green) and calbindin (red), a marker for Purkinje cells, in primary cultures of embryonic mouse cerebellar neurons *in vitro*. c-Met-immunoreactivity (IR) was observed in a large number of cerebellar neurons, with most of these presumably being granular cells. In addition to these neurons, c-Met-IR was indeed detected in calbindin-positive Purkinje cells (Fig. 1A).

3.2. c-Met is expressed in the cerebellar Purkinje cells and Bergmann glia in vivo

We next assessed whether c-Met is expressed in Purkinje cells *in vivo* using double immunostaining for c-Met (red) and calbindin (green) in the cerebella of WT mice. c-Met-IR was detected in Purkinje cells of the cerebella of WT mice. In addition, c-Met-IR was detected in other cells surrounding to the Purkinje cells (Fig. 1B). These cells that were closely apposed to Purkinje cells resembled Bergmann glia. To determine if these non-Purkinje cells were Bergmann glia, double immunostaining for c-Met (red) and GFAP (green), a marker for Bergmann glia, was performed. As shown in Fig. 1C, c-Met-IR was detected in Bergmann glia. These findings

indicate that both Purkinje cells and Bergmann glia are potential target cells of HGF *in vivo*.

3.3. Immunohistochemical analyses of HGF and phospho-c-Met in the cerebellum of WT, HGF-Tg, SCA7-KI, and SCA7-KI/HGF-Tg mice

To explore whether HGF can modify the degeneration of Purkinje cells in SCA7-KI mice, we used neuron-specific enolase (NSE)-driven HGF overexpression transgenic mice (HGF-Tg) to introduce HGF into the Purkinje cells of SCA7-KI mice. Crossing SCA7-KI mice with HGF-Tg mice generated the following four mouse models: (1) wild-type littermates (WT), (2) HGF-Tg, (3) SCA7-KI, and (4) SCA7-KI/HGF-Tg mice. This approach allowed the stable introduction of the HGF gene directly into the cerebellar neurons of SCA7-KI mice. Confirmation that HGF was introduced into the cerebellum of SCA7-KI/HGF-Tg mice was accomplished with immunostaining. HGF-IR was faintly detected in calbindin-positive Purkinje cells and GFAP-positive Bergman glia of the cerebellum in WT and SCA7-KI mice (Fig. 2A, upper panel), while more intense staining of HGF-IR was detected in Purkinje cells of HGF-Tg mice as well as in SCA7-KI/HGF-Tg mice (Fig. 2A, bottom panel). In addition to Purkinje cells, HGF-IR was detected in cells surrounding the Purkinje cells, *i.e.* GFAP-positive Bergmann glia. These findings were further confirmed by quantitative analyses of the immunofluorescent intensity of HGF-IR in sections of the cerebellum (Fig. 2B) and HGF content using ELISA analyses (Fig. 2C). These findings suggest that overexpressed HGF in cerebellar neurons is released into the extracellular space, and is in turn distributed to Bergmann glia.

3.4. c-Met is tyrosine-phosphorylated in Purkinje cells and Bergmann glia in SCA7-KI/HGF-Tg mice

Further attempts were made to determine if overexpression of HGF contributes to tyrosine-phosphorylation, and thereby activation, of c-Met in SCA7-KI/HGF-Tg mice. The level of phospho-c-Met-IR was much higher in both the Purkinje cells and Bergmann glia of SCA7-KI/HGF-Tg mice compared to those of SCA7-KI mice. These findings demonstrate that overexpression of HGF in SCA7-KI/HGF-Tg mice contributes to the activation of c-Met in Purkinje cells and Bergmann glia, prompting an examination of the role of HGF in the modulation of these cells in SCA7-KI mice (Fig. 2D).

3.5. Overexpression of HGF attenuates the degeneration of Purkinje cells of the cerebellum in SCA7-KI mice

To elucidate whether HGF plays a role in attenuating the degeneration of Purkinje cells in SCA7-KI mice, we next compared the morphology of Purkinje cells from the cerebella of SCA7-KI and SCA7-KI/HGF-Tg mice. Calbindin immunohistochemistry revealed that Purkinje cells appeared to have large spherical cell bodies in both WT and HGF-Tg mice, while a number of Purkinje cells with reduced cellular size (degenerated neurons, white arrowheads), were present in SCA7-KI mice (Fig. 3A). In contrast, many more large spherical neurons were observed in SCA7-KI/HGF-Tg mice compared to SCA7-KI mice (Fig. 3A). The size distribution of Purkinje cells in WT, HGF-Tg, SCA7-KI, and SCA7-KI/HGF-Tg mice is shown in Fig. 3B. Quantitative analyses showed that the size of Purkinje cells in SCA7-KI mice was varied from small (<150 μm^2) to large (>150 μm^2; healthy), while the quantity of small Purkinje cells (<150 μm^2) was reduced in SCA7-KI/HGF-Tg mice (Fig. 3B). Namely, the fraction of small Purkinje cells was significantly lower in SCA7-KI/HGF-Tg mice than in SCA7-KI mice. These findings demonstrate that overexpression of HGF attenuates the degeneration of Purkinje cells in SCA7-KI mice.

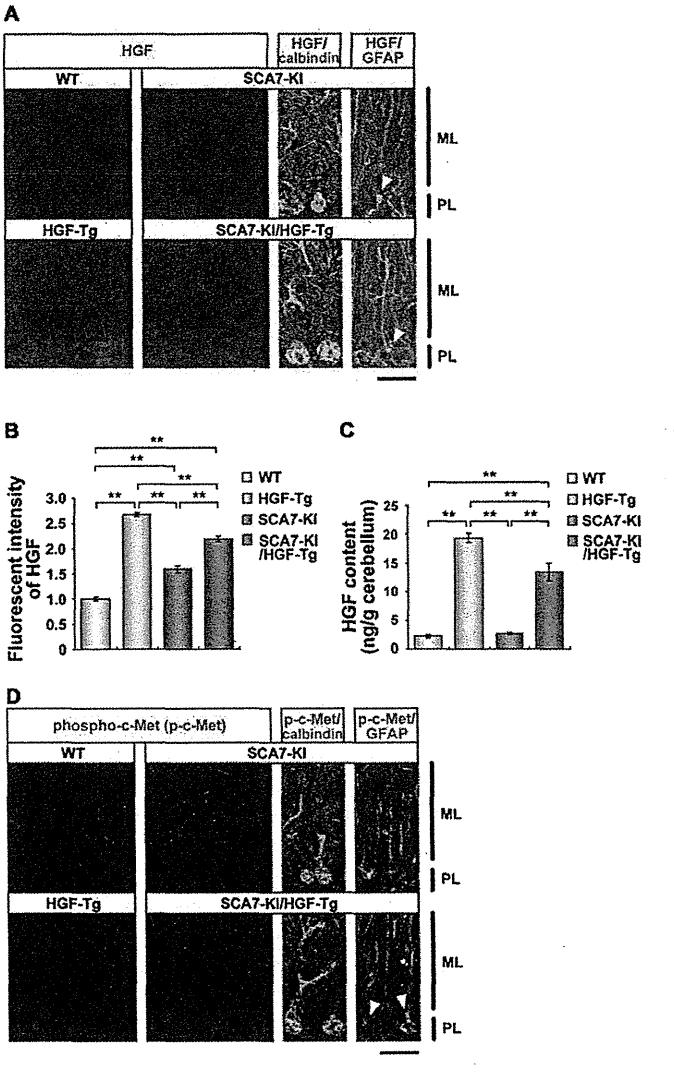

Fig. 2. Immunohistochemical localization of HGF and phospho-c-Met in cerebellar cells *in vivo*. Comparison of HGF levels by immunohistochemistry (A and B) and HGF ELISA (C) in the cerebellum of 10-week-old WT, HGF-Tg, SCA7-KI, and SCA7-KI/HGF-Tg mice using anti-rat HGF that detects both endogenous and exogenous (overexpressed) HGF proteins. (A) HGF-IR is elevated in HGF-Tg and SCA7-KI/HGF-Tg mice. PL, Purkinje cell layer; ML, molecular layer. Bar, 30 μm. White arrowhead indicates GFAP/HGF double-positive cells. (B) Fluorescent intensity ($n = 6$ per group) of HGF in each group. Mean HGF signal intensity was significantly elevated compared to WT (**$P < 0.01$, Fisher's PLSD test). Error bars indicate S.E.M. (C) HGF protein levels in the whole cerebellum are elevated in HGF-Tg and SCA7-KI/HGF-Tg mice ($n = 4$ per group, **$P < 0.01$, Fisher's PLSD test). Error bars indicate S.E.M. (D) Immunohistochemistry of tyrosine phosphorylation at positions 1230, 1234, and 1235 of c-Met (phospho-c-Met, red) in the cerebellum in 10-week-old mice. Phospho-c-Met staining is shown in the cerebellum in all mice groups. Phospho-c-Met-IR is elevated in both Purkinje cells (lower left panel, green) and Bergmann glia (lower right panel, green) of SCA7-KI/HGF-Tg mice compared to SCA7-KI mice (upper panel, green). White arrowheads indicate GFAP/phospho-c-Met double-positive cells. Bar, 30 μm. (For interpretation of the references to color in this figure caption, the reader is referred to the web version of the article.)

3.6. Overexpression of HGF maintains the levels of the glutamate transporters (GLAST and GLT-1) in the cerebellum of SCA7-KI mice

Bergmann glia are responsible for glutamate uptake (removal) from the Purkinje cell synaptic cleft. It has been suggested that polyglutamine-expanded ataxin-7 induces Purkinje cell excitotoxicity by interfering with Bergmann glia-mediated glutamate uptake. This is due to the fact that the expression of GLAST, a

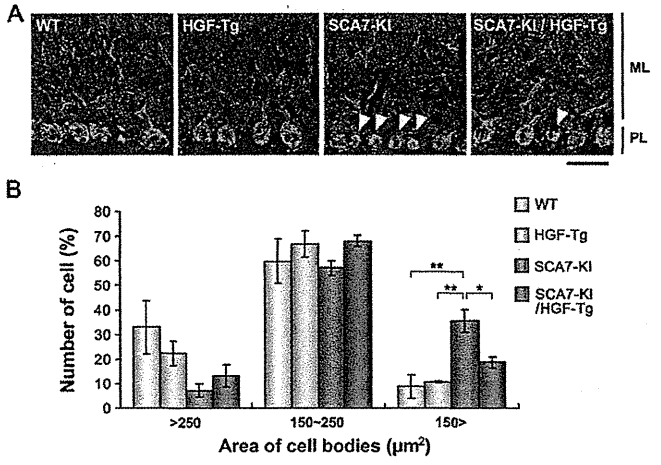

Fig. 3. HGF attenuates degeneration of Purkinje cell bodies. (A) Immunohistochemistry of calbindin (green) in the cerebellum of 10-week-old mice. SCA7-KI mice displayed smaller Purkinje cell body size than WT and HGF-Tg mice. SCA7-KI/HGF-Tg mice showed an attenuation of shrinkage of Purkinje cell bodies. PL, Purkinje cell layer; ML, molecular layer. Bar, 30 μm. White arrowhead indicates degenerative Purkinje cell changes. (B) Quantification of cell numbers with different Purkinje cellular body size (>250; 150–250; <150 μm^2) of each group ($n = 3$ per group). The number of small cells (area are less than 150 μm^2) in SCA7-KI mice is significantly greater *versus* WT and HGF-Tg mice (**$P < 0.01$, Fisher's PLSD test), SCA7-KI/HGF-Tg mice exhibit significantly fewer small cells compared to SCA7-KI mice (*$P < 0.05$). Error bars indicate S.E.M. (For interpretation of the references to color in this figure caption, the reader is referred to the web version of the article.)

glutamate transporter in the cerebellum, is confined to Bergmann glia and marked reductions in GLAST expression (and glutamate uptake) have been observed in presymptomatic Gfa2-SCA7-92Q mice (Custer et al., 2006). As c-Met is expressed in the Bergmann glia of WT mice and is phosphorylated (*i.e.* activated) in Bergmann glia in SCA7-KI/HGF-Tg mice (Figs. 1C and 2D), we next examined whether HGF affects the morphology and function of Bergmann glia. Immunostaining for GFAP revealed that obvious morphological difference of Bergmann glia was not detected between WT mice and SCA7-KI/HGF-Tg mice (Fig. 4A). We then examined whether HGF modulates the down-regulation of GLAST levels in SCA7-KI mice. Immunostaining for GLAST revealed that GLAST levels were decreased in SCA7-KI mice compared to WT mice, while the levels were generally maintained in SCA7-KI/HGF-Tg mice (Fig. 4B and C). These findings demonstrate that HGF supports GLAST levels in SCA7-KI mice. We then examined HGF regulation of GLT-1, another glutamate transporter that is also abundant in the cerebellum, by a similar mechanism. Immunostaining for GLT-1 revealed that the levels of GLT-1 were markedly decreased in SCA7-KI mice compared to WT mice, while the level was maintained or even increased in SCA7-KI/HGF-Tg mice (Fig. 4D and E). These findings demonstrate that HGF maintains or even increases the levels of GLT-1 in SCA7-KI mice.

3.7. *Overexpression of HGF improves rotarod performance in SCA7-KI mice*

Data obtained so far suggested that SCA7 could be improved by HGF *via* the attenuation of Purkinje cellular degeneration and reduction of glutamate transporters in Bergmann glia. Therefore, we examined whether these improvements were reflected by

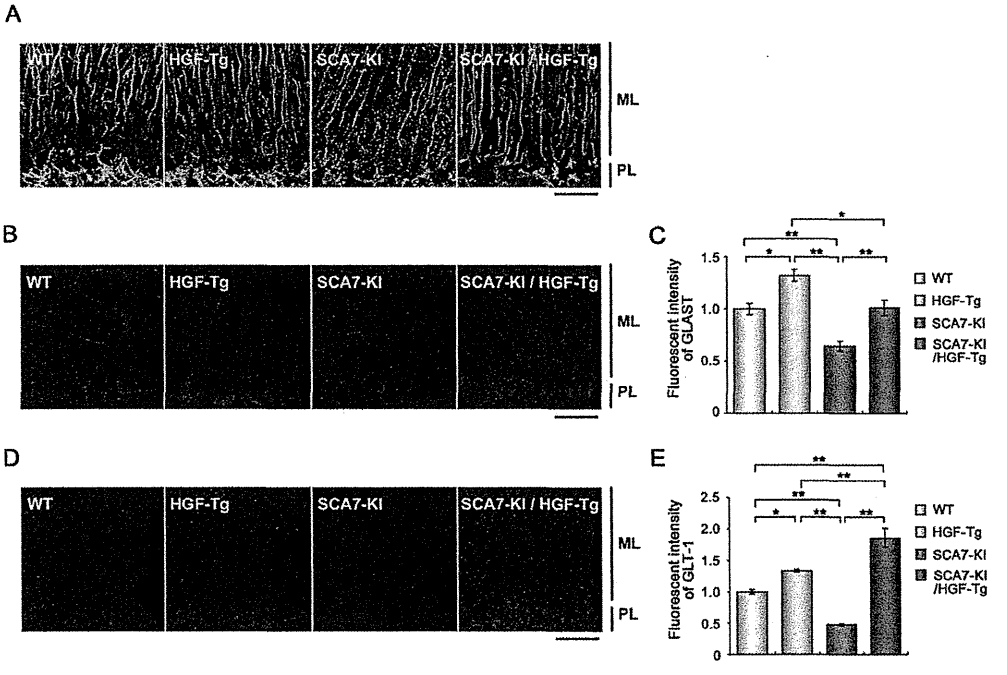

Fig. 4. HGF maintains the levels of glutamate transporters (GLAST and GLT-1) in Bergmann glia in the cerebellum of SCA7-KI mice. (A) Immunohistochemistry for Bergmann glia (GFAP, green) in the cerebellum in 10-week-old mice. No significant alterations were detected in the morphology of Bergmann glia. PL, Purkinje cell layer; ML, molecular layer. Bar, 30 μm. (B and C) Comparison of GLAST levels in 10-week-old mice. (B) Immunohistochemistry for GLAST in the cerebellum. GLAST staining is reduced in the SCA7-KI mouse cerebellum and is significantly rescued in the SCA7-KI/HGF-Tg cerebellum. Bar, 30 μm. (C) Quantification of fluorescent intensity ($n = 3$ per group) of PL. Mean GLAST signal intensity is significantly elevated in SCA7-KI/HGF-Tg cerebellum *versus* SCA7-KI cerebellum (*$P < 0.05$, **$P < 0.01$, Fisher's PLSD test). Error bars indicate S.E.M. (D and E) Comparison of GLT-1 level at 10-week-old mice. (D) Immunohistochemistry for GLT-1 in the cerebellum. GLT-1 staining is reduced in the cerebellum of SCA7-KI mice, while significantly elevated in the cerebellum of SCA7-KI/HGF-Tg mice. Bar, 30 μm. (E) Mean fluorescent intensity ($n = 3$ per group) of PL. Mean GLT-1 signal intensity is significantly elevated in the cerebellum of SCA7-KI/HGF-Tg mice (*$P < 0.05$, **$P < 0.01$, Fisher's PLSD test). Error bars indicate S.E.M. (For interpretation of the references to color in this figure caption, the reader is referred to the web version of the article.)

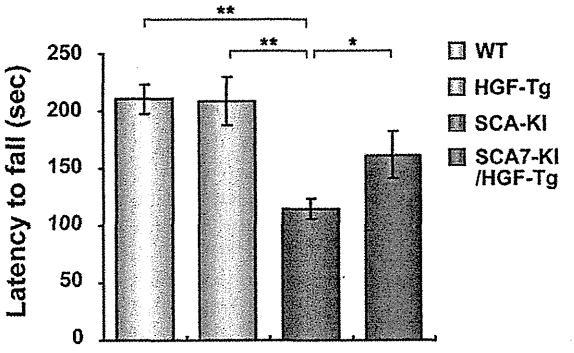

Fig. 5. HGF improves coordinated motor behavior of SCA7-KI mice. Comparison of motor coordination in 10-week-old WT, HGF-Tg, SCA7-KI, and SCA7-KI/HGF-Tg mice using the rotarod test. SCA7-KI/HGF-Tg mice display improved rotarod performance compared to SCA7-KI mice ($n = 8–12$ per group; $^*P < 0.05$, $^{**}P < 0.01$, Student's t test). Error bars indicate S.E.M.

motor performance of WT, HGF-Tg, SCA7-KI, and SCA7-KI/HGF-Tg mice. To examine the ability of an animal to balance on a rotating rod, rotarod tests were applied on each animal at 10 weeks of age. There was a marked reduction in the latency to fall in SCA7-KI mice compared to WT and HGF-Tg mice. However, the latency to fall of SCA7-KI/HGF-Tg mice was significantly longer than that of SCA7-KI mice (Fig. 5), suggesting that overexpression of HGF contributes to the amelioration of rotarod performance impairments in SCA7-KI mice.

4. Discussion

In the present study, we examined whether overexpression of HGF, a pleiotrophic growth factor with highly potent neurotrophic activities, exhibits a beneficial function in SCA7-KI mice. By crossing SCA7-KI mice with HGF-Tg mice that overexpress HGF under the NSE promoter, four groups of mice (WT, HGF-Tg, SCA7-KI, and SCA7-KI/HGF-Tg mice) were generated. The results indicate that overexpression of HGF attenuates the degeneration of Purkinje cells, maintains the levels of the glutamate transporters GLAST and GLT-1 in Bergmann glia and improves rotarod performance deficits observed in SCA7-KI mice.

The molecular mechanisms responsible for these events have not yet been clarified in detail. However, because HGF protein is expressed and distributed in Purkinje cells and Bergmann glia in SCA7-KI/HGF-Tg mice at much higher levels than in SCA7-KI mice, and because the expression and phosphorylation (activation) of c-Met was observed at much higher levels in both the Purkinje cells and Bergmann glia of SCA7-KI/HGF-Tg mice, it seems likely that HGF functions directly on Purkinje cells as well as Bergmann glia. If there is a direct interaction, the ability of HGF to function not only on Purkinje cells but also on Bergmann glia might represent a therapeutic opportunity for attenuating the degeneration of Purkinje cells, since recent genetic approaches suggest that an important mutual interaction of Purkinje cells and Bergmann glia in SCA7 might, at least in part, be involved in the degeneration of these cells in this disease (Custer et al., 2006; Furrer et al., 2011). Furthermore, Bergmann glia are also shown to secrete neurotrophic factors that support Purkinje cells (Mount et al., 1995).

Purkinje cells are integrated into a complex neural network and receive glutamatergic input from axons projecting from the inferior olive and cerebellar granule cells. Hence, in addition to Purkinje cells and Bergmann glia, which we focused on the present study, other cells and their neural networks in the cerebellum may also play a role in the pathogenesis of disease models of SCA7 and related diseases (Gatchel et al., 2007; Furrer et al., 2011). For example, transcriptional down-regulation of insulin-like growth factor binding protein 5 (*igfbp5*) in cerebellar granule cells is proposed to be involved in non-cell-autonomous degeneration of Purkinje cells in SCA7-KI mice (Gatchel et al., 2007). It has not yet been determined whether HGF could alleviate reduction of *igfbp5*, and this possibility is worth examining in a future study. Given that HGF elicits neurotrophic activity on cerebellar granular cells both *in vitro* and *in vivo* (Zhang et al., 2000; Ieraci et al., 2002), we cannot exclude the possibility that HGF functions on granular cells and alleviates the down-regulation of *igfbp5*. Therefore, HGF may also contribute to attenuation of Purkinje cell degeneration *via* cerebellar granular cells.

It has not yet been determined whether HGF alleviates the degeneration of the retina, the other region associated with phenotypic changes appearing in SCA7-KI mice. HGF and c-Met are expressed in various populations of rat retinal neurons during development as well as in the adult, and neuroprotective effects of HGF on rat retinal photoreceptors have been reported (Machida et al., 2004; Ohtaka et al., 2006; Shibuki et al., 2002; Sun et al., 1999).

The rotarod test is used to analyze motor phenotype, in the aspect of motor balance and/or its coordination (Carter et al., 2001; Custer et al., 2006). Hence, the ability of HGF to improve rotarod performance raises the potential utility of HGF for the improvement of motor impairment of affected individuals. However, further experiments are required to address the relationship between the outcome of rotarod tests in the present study and the clinical ataxic phenotype of SCA7.

Cvetanovic et al. (2011) recently reported that genetic overexpression or pharmacologic infusion of recombinant vascular endothelial growth factor (VEGF) ameliorates the ataxic phenotype and degeneration of Purkinje cells in a mouse model of another type of spinocerebellar ataxia, spinocerebellar ataxia type 1 (SCA1). Given that HGF promotes angiogenesis in a variety of disease models (Funakoshi and Nakamura, 2003, 2011) and that c-Met is not only expressed in Purkinje cells and Bergmann glia but also in other types of cells including vascular cells and neural progenitor populations in WT mice (Funakoshi and Nakamura, 2011; Noma et al., unpublished results), it would be interesting to know how HGF plays a role in SCA1-model mice and whether HGF promotes angiogenesis and neurogenesis in SCA7-KI mice. It should be noted that exercise produces beneficial effects in alleviating SCA1 symptoms in mice (Fryer et al., 2011). Exercise is known to promote HGF production in some patients (Yasuda et al., 2004) and that HGF improves the phenotype of SCA7-KI as shown in the present study. Hence, it would also be interesting to examine whether exercise plays a role in the attenuation of the progression of the course of SCA7-KI pathology and if HGF is involved in the process.

In summary, the present study provided the first evidence that overexpression of HGF is beneficial for attenuating the degeneration of both Purkinje cells and Bergmann glia. Considered with the notion that intrathecal injection of recombinant human HGF protein has been shown to be effective in several disease models, such as a transgenic rat model of ALS (Ishigaki et al., 2007) and a primate model of spinal cord injury (Kitamura et al., 2011), our findings may raise the possibility of a therapeutic use of HGF in SCA7 and related disorders.

Acknowledgements

This work was supported in part by Grants-in-Aid from the Ministry of Health, Labour and Welfare of Japan and Grants-in-Aid from the Ministry of Education, Science, and Culture of Japan. We wish to thank Prof. Huda Y. Zoghbi for providing us the SCA7-KI mice. We are grateful to Ms. Higano, Ms. Ikushima and Ms. Yoneda for secretarial assistance.

References

Carter, R.J., Morton, J., Dunnett, S.B., 2001. Motor coordination and balance in rodents. Curr. Protoc. Neurosci. (Chapter 8): Unit 8.12.

Custer, S.K., Garden, G.A., Gill, N., Rueb, U., Libby, R.T., Schultz, C., Guyenet, S.J., Deller, T., Westrum, L.E., Sopher, B.L., La Spada, A.R., 2006. Bergmann glia expression of polyglutamine-expanded ataxin-7 produces neurodegeneration by impairing glutamate transport. Nat. Neurosci. 9, 1302–1311.

Cvetanovic, M., Patel, J.M., Marti, H.H., Kini, A.R., Opal, P., 2011. Vascular endothelial growth factor ameliorates the ataxic phenotype in a mouse model of spinocerebellar ataxia type 1. Nat. Med. 17, 1445–1447.

Fryer, J.D., Yu, P., Kang, H., Mandel-Brehm, C., Carter, A.N., Crespo-Barreto, J., Gao, Y., Flora, A., Shaw, C., Orr, H.T., Zoghbi, H.Y., 2011. Exercise and genetic rescue of SCA1 via the transcriptional repressor Capicua. Science 334, 690–693.

Funakoshi, H., Nakamura, T., 2003. Hepatocyte growth factor: from diagnosis to clinical applications. Clin. Chim. Acta 327, 1–23.

Funakoshi, H., Nakamura, T., 2011. Hepatocyte growth factor (HGF): neurotrophic functions and therapeutic implications for neuronal injury/diseases. Curr. Signal Transduct. Ther. 6, 156–167.

Furrer, S.A., Mohanachandran, M.S., Waldherr, S.M., Chang, C., Damian, V.A., Sopher, B.L., Garden, G.A., La Spada, A.R., 2011. Spinocerebellar ataxia type 7 cerebellar disease requires the coordinated action of mutant ataxin-7 in neurons and glia, and displays non-cell-autonomous Bergmann glia degeneration. J. Neurosci. 31, 16269–16278.

Huang, H., Bordey, A., 2004. Glial glutamate transporters limit spillover activation of presynaptic NMDA receptors and influence synaptic inhibition of Purkinje neurons. J. Neurosci. 24, 5659–5669.

Honda, S., Kagoshima, M., Wanaka, A., Tohyama, M., Matsumoto, K., Nakamura, T., 1995. Localization and functional coupling of HGF and c-Met/HGF receptor in rat brain: implication as neurotrophic factor. Brain Res. Mol. Brain Res. 32, 197–210.

Hossain, M.A., Russell, J.C., Gomez, R., Laterra, J., 2002. Neuroprotection by scatter factor/hepatocyte growth factor and FGF-1 in cerebellar granule neurons is phosphatidylinositol 3-kinase/akt-dependent and MAPK/CREB-independent. J. Neurochem. 81, 365–378.

Ieraci, A., Forni, P.E., Ponzetto, C., 2002. Viable hypomorphic signaling mutant of the Met receptor reveals a role for hepatocyte growth factor in postnatal cerebellar development. Proc. Natl. Acad. Sci. U.S.A. 99, 15200–15205.

Ishigaki, A., Aoki, M., Nagai, M., Warita, H., Kato, S., Kato, M., Nakamura, T., Funakoshi, H., Itoyama, Y., 2007. Intrathecal delivery of hepatocyte growth factor from amyotrophic lateral sclerosis onset suppresses disease progression in rat amyotrophic lateral sclerosis model. J. Neuropathol. Exp. Neurol. 66, 1037–1044.

Kadoyama, K., Funakoshi, H., Ohya, W., Nakamura, T., 2007. Hepatocyte growth factor (HGF) attenuates gliosis and motoneuronal degeneration in the brainstem motor nuclei of a transgenic mouse model of ALS. Neurosci. Res. 59, 446–456.

Kitamura, K., Fujiyoshi, K., Yamane, J., Toyota, F., Hikishima, K., Nomura, T., Funakoshi, H., Nakamura, T., Aoki, M., Toyama, Y., Okano, H., Nakamura, M., 2011. Human hepatocyte growth factor promotes functional recovery in primates after spinal cord injury. PLoS One 6, e27706.

Machida, S., Tanaka, M., Ishii, T., Ohtaka, K., Takahashi, T., Tazawa, Y., 2004. Neuroprotective effect of hepatocyte growth factor against photoreceptor degeneration in rats. Invest. Ophthalmol. Vis. Sci. 45, 4174–4182.

Miyazawa, T., Matsumoto, K., Ohmichi, H., Katoh, H., Yamashima, T., Nakamura, T., 1998. Protection of hippocampal neurons from ischemia-induced delayed neuronal death by hepatocyte growth factor: a novel neurotrophic factor. J. Cereb. Blood Flow Metab. 18, 345–348.

Mount, H.T., Dean, D.O., Alberch, J., Dreyfus, C.F., Black, I.B., 1995. Glial cell line-derived neurotrophic factor promotes the survival and morphologic differentiation of Purkinje cells. Proc. Natl. Acad. Sci. U.S.A. 92, 9092–9096.

Nakamura, T., Nawa, K., Ichihara, A., 1984. Partial purification and characterization of hepatocyte growth factor from serum of hepatectomized rats. Biochem. Biophys. Res. Commun. 122, 1450–1459.

Nakamura, T., Nishizawa, T., Hagiya, M., Seki, T., Shimonishi, M., Sugimura, A., Tashiro, K., Shimizu, S., 1989. Molecular cloning and expression of human hepatocyte growth factor. Nature 342, 440–443.

Ohtaka, K., Machida, S., Ohzeki, T., Tanaka, M., Kurosaka, D., Masuda, T., Ishii, T., 2006. Protective effect of hepatocyte growth factor against degeneration of the retinal pigment epithelium and photoreceptor in sodium iodate-injected rats. Curr. Eye Res. 31, 347–355.

Ohya, W., Funakoshi, H., Kurosawa, T., Nakamura, T., 2007. Hepatocyte growth factor (HGF) promotes oligodendrocyte progenitor cell proliferation and inhibits its differentiation during postnatal development in the rat. Brain Res. 1147, 51–65.

Shibuki, H., Katai, N., Kuroiwa, S., Kurokawa, T., Arai, J., Matsumoto, K., Nakamura, T., Yoshimura, N., 2002. Expression and neuroprotective effect of hepatocyte growth factor in retinal ischemia-reperfusion injury. Invest. Ophthalmol. Vis. Sci. 43, 528–536.

Sun, W., Funakoshi, H., Nakamura, T., 1999. Differential expression of hepatocyte growth factor and its receptor, c-Met in the rat retina during development. Brain Res. 851, 46–53.

Sun, W., Funakoshi, H., Nakamura, T., 2002. Overexpression of HGF retards disease progression and prolongs life span in a transgenic mouse model of ALS. J. Neurosci. 22, 6537–6548.

Yamada, A., Matsumoto, K., Iwanari, H., Sekiguchi, K., Kawata, S., Matsuzawa, Y., Nakamura, T., 1995. Rapid and sensitive enzyme-linked immunosorbent assay for measurement of HGF in rat and human tissues. Biomed. Res. 16, 105–114.

Yasuda, S., Goto, Y., Takaki, H., Asaumi, Y., Baba, T., Miyazaki, S., Nonogi, H., 2004. Exercise-induced hepatocyte growth factor production in patients after acute myocardial infarction: its relationship to exercise capacity and brain natriuretic peptide levels. Circ. J. 68, 304–307.

Yoo, S.Y., Pennesi, M.E., Weeber, E.J., Xu, B., Atkinson, R., Chen, S., Armstrong, D.L., Wu, S.M., Sweatt, J.D., Zoghbi, H.Y., 2003. SCA7 knockin mice model human SCA7 and reveal gradual accumulation of mutant ataxin-7 in neurons and abnormalities in short-term plasticity. Neuron 37, 383–401.

Zhang, L., Himi, T., Morita, I., Murota, S., 2000. Hepatocyte growth factor protects cultured rat cerebellar granule neurons from apoptosis via the phosphatidylinositol-3 kinase/Akt pathway. J. Neurosci. Res. 59, 489–496.

ウイルス肝炎のすべて

Ⅲ　血液感染するウイルス肝炎

1．B型肝炎

（1）B型肝炎のウイルス学

上田 啓次*

1960年代にBlumbergがオーストラリア抗原と肝炎との関連を示してから半世紀が迫ろうとしている。この抗原こそがB型肝炎ウイルス(hepatitis B virus：HBV)の遺伝子産物であった。分子生物学の発展とともに，HBVの塩基配列の決定，遺伝子同定，遺伝子機能の解析は進み，ワクチンの開発にも成功した。しかしながら，簡便な感染系が存在しないことからHBVのウイルス学はまったく進展しておらず，HBVの真のライフサイクルのみならず，急性あるいは慢性肝炎，肝硬変，肝がんといった深刻な病態の発症機構は不明な点が多い。問題解決にはHBV感染受容体を分離・同定し，確固とした，かつ簡便な感染系を樹立することが不可欠である。ウイルス学最大の難問を解決する糸口を模索する。

Key Words：hepatitis B virus，HBV，逆転写，感染受容体，感染系

Ⅰ はじめに

Blumbergが白血病患者血清中に新規の抗原(オーストラリア抗原)を発見し報告したのは1965年[1]，その後，数年で輸血後の血清肝炎との関連が確立された[2]。この感染性因子がB型肝炎ウイルス（hepatitis B virus：HBV)である。わが国では大河内らが最初に，日本人における本抗原の保有率を報告している[3]。疾患概念の確立は，慢性B型肝炎から肝硬変，肝がんへの病態進行や母体からの垂直感染の存在を明らかにした。

1970年代後半～80年代前半にかけて，分子生物学的研究手法の確立と相まって，次々とウイルスゲノムのクローニングと塩基配列が決定され，げっ歯類のウッドチャック(woodchuck hepatitis virus：WHV)や地リス（ground squirrel hepatitis virus：GSHV)，鳥類ではアヒル（duck hepatitis B virus：DHBV）や鷺（heron hepatitis B virus）にも同族のウイルスが存在することが明らかにされた。哺乳類では類人猿であるチ

Viorology of the hepatitis B virus

*大阪大学大学院医学系研究科感染免疫医学講座ウイルス学 教授　*Keiji Ueda*

ンパンジー (chimpanzee hepatitis B virus) やオランウータン (orangutan hepatitis B virus) などにも同様のヘパドナウイルスが蔓延していることが知られている[4) 5)]。

また, HBVは従来, サブタイプとしてadr, adw, aywのように分類されていたが, 最近ではゲノタイプA～Hとして分類されている[4)]。

ヘパドナウイルスの特徴は, ゲノムサイズがきわめて小さく, およそ3.2kb前後の部分的2本鎖の環状DNAウイルスであること, 遺伝子は大まかに言って, コア遺伝子, pol遺伝子, S遺伝子とX遺伝子のたった4つである (鳥類のヘパドナウイルスにはX遺伝子は存在しないとされている) ことや, DNAウイルスでありながら複製に逆転写過程が存在することである[4) 5)]。

分子生物学的手法により各遺伝子の機能や複製機構, 組み込み体の解析から肝がん発生との関連が研究されてきた。しかしながら, ヘパドナウイルス学を論じる上で解決されていない決定的な問題が2つあり, その問題が解決されない限り, ヘパドナウイルスの真のウイルス学, 病態論やウイルスの本質に則した治療法の開発はないものと考えている。その問題点とは, 有用かつ簡便な感染系が存在しないこと, ヘパドナウイルス複製酵素polの*in vitro*アッセイ系が存在しないことである。

本稿ではHBVを概説した後, 前述の解決されない主要2問題について概説したい。

Ⅱ HBV粒子構造, ゲノム, 遺伝子, 転写産物

HBVの感染性粒子はDane粒子と呼ばれる膜粒子とその内部のコア粒子(キャプシド)で構成され, キャプシド内にウイルスゲノムを内在する (**図1A**)。前述のごとく, HBVのゲノムはきわめてコンパクトに組織されている。また, 単純な2本鎖DNAゲノムではなく, 部分的に2本鎖の環状DNAである。さらに, ⊖鎖DNAの5'端に末端タンパクが付着し, ⊕鎖DNAの5'にはプライマーRNAがついているという独特の構造をしている (**図1B**)。また, レトロウイルスゲノム末端の非翻訳領域 (untranslated region：**UTR**) に機能的に相同と考えられるdirect repeat 1および2 (DR1, DR2) 配列がある。DR1はプレゲノムRNAの5'に, 3'にはDR2およびDR1が存在している[4)]。

このきわめてコンパクトなゲノムにウイルスとしての営みに必要な最小限の遺伝子がコードされている。それらの遺伝子は, コア (C), pol, SとX遺伝子の4つである。コア遺伝子とS遺伝子は読み取り枠の違いにより, コア遺伝子はpreC-CとCの2つに, また, S遺伝子はlarge S (LS), middle S (MS), small S (SS) の3つに分けられる (**図1**)。

Ⅲ preC-C (プレコアーコア) 遺伝子

ウイルスのキャプシド形成にかかわる構造遺伝子産物を供給する。2つのin-frame翻訳コドンにより, preC (29アミノ酸〔aa〕)-C (185aa) の読み取り枠となるか, Cのみの読み取り枠となるかが決定される。PreC-CあるいはC遺伝子に固有の転写産物はないが, preC-Cの読み取り枠になるにはpreC-C翻訳開始コドンATGより上流から転写が開始される必要がある。また, Cの翻訳にかかわる転写産物は, いわゆるプレゲノムRNAと考えられる (**図2A**)。

PreC-C産物はN末に疎水性アミノ酸配列からなる分泌シグナルがあり, また, C末のアルギニンに富む領域の前で切断されてHBe抗原として分泌される[4)]。HBe抗原産生のウイルスにとっての生理的な意義はよくわからないが, C遺伝子産物とほとんどオー

HBV (hepatitis B virus；B型肝炎ウイルス)　UTR (untranslated region；非翻訳領域)

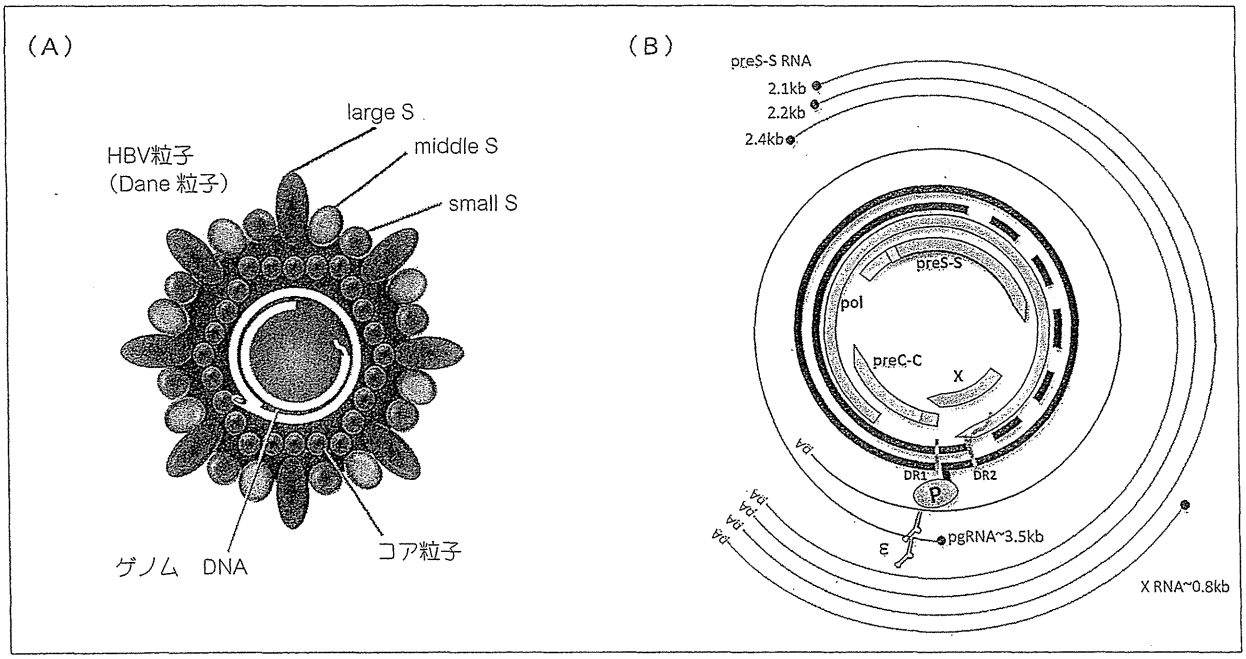

図1 HBV粒子とゲノム構造

(A) HBVの感染性粒子構造。HBVは部分2重鎖DNA環状構造をもつゲノムを内在するコア粒子（キャプシッド）と，それを被う外膜構造をもつ。外膜は，LS，MS，SSで構成される。(B) HBVゲノム（太い実線，部分2重鎖は破線）の構造，関連転写産物（外枠：細い実線），遺伝子（タンパク読み取り枠）（内側：ブロック矢印）を示す。ゲノムは⊖鎖5'に末端タンパク（P）（HBV pol）が付着している。複製に重要なDR（direct repeat）1，DR2の位置が示されている。転写産物の5'はcap構造を取り（●）ポリAで終わる。3.5kb mRNAは正確にはpreC-C産生にかかわるpreC ATGを含むものと，含まないプレゲノムRNA（pgRNA）に分けられる。pgRNAについてのみ，εの位置，構造を示してある。preS-S産生にかかわるmRNAは，2.4kb（LS），2.2kb（MS），2.1kb（SS）である。また，0.8kb mRNAはX遺伝子固有のmRNAである。

HBV：B型肝炎ウイルス （文献4より）

バーラップしていることから，キャリア化や慢性肝炎化などの持続性HBV感染に起因している可能性があると思われる。

血中HBe抗原の量はHBV慢性肝炎の活動性ともよく関連し，HBV増殖状況をよく反映している。HBe抗原陰性化とHBe抗体の陽性化というseroconversionにpreC領域内の終始コドンへの変異をともなうことが知られており，これにともない，肝炎も鎮静化することが多い[6]。

C遺伝子産物はHBVのコア粒子形成に不可欠なタンパク因子である。2量体が集合して最終的なコア粒子を形成すると考えられている。単一構成因子であるため，T（T；triangulation number）＝1のもっとも単純な正二十面体キャプシドを形成すると予測されるが，cryoelectronmicroscopyによる粒子結晶構造解析ではT＝3～4で，約180～240分子からなる正二十面体構造をとっていることがわかっている[7]。

コア粒子の形成過程でパッケージングシグナルεを介してプレゲノムRNAが粒子に取り込まれ，あるいはコアタンパクの分子集合に付随しつつ，プレゲノムRNAから逆転写により⊖鎖DNA合成，そして⊕鎖DNA合成が進行するものと考えられる[8]。コアタンパクが核内に存在することは報告されているが，コア粒子そのものがどこで形成され，どのような過程で膜粒子に取込まれるかなど，ウイルス粒子形成のダイナミックな分子集合プロセスには不明な点が多い。

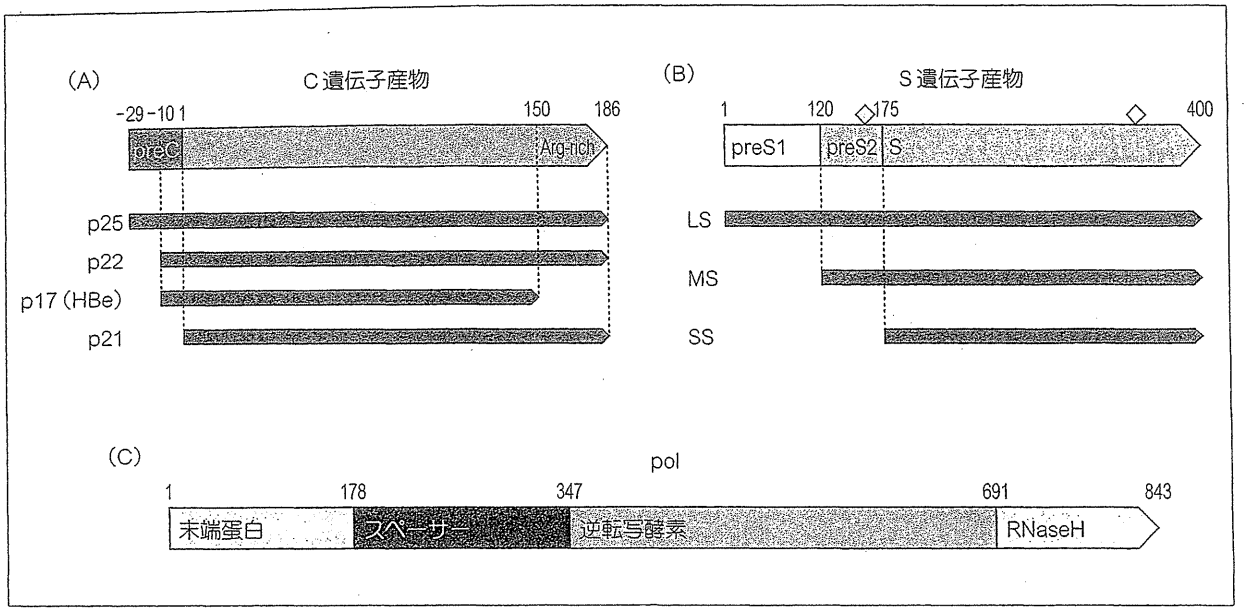

図2 コア (C), S, pol の産物と機能領域

(A) C 遺伝子産物。読み取り枠は preC-C と C の2つであるが，実際発現されるタンパクは最低4種類あると考えられている。p25 は preC-C の前駆体として発現し，N 端の分泌シグナル (−29 ～−9aa) (p22) と 150aa 以降のアルギニンに富む領域がプロセスされて p17 として分泌される。コア粒子の産生には p21 がかかわると考えられる。(B) S 遺伝子産物。SS 部分を共通として preS2 が加わった MS，さらに preS1 が加わった LS が産生される。preS2 と SS の C 端の◇は糖鎖付加部分を示す。(C) HBV pol タンパクの機能構造。N 端からタンパクプライミング逆転写にかかわる末端タンパク，機能領域を連結させるスペーサー，酵素活性を担う逆転写酵素領域，RNA 分解反応にかかわる RNaseH 領域からなる。

(文献5より)

Ⅳ pol

HBV ゲノム複製の根幹的役割を果たす因子である。845aa 前後からなり，末端タンパク領域，tethering 領域（もしくは spacer 領域），逆転写酵素活性領域，RNaseH 領域という各ドメインから構成されると考えられる（**図2B**）。前述のコアタンパクにはレトロウイルスの gag-pol 融合タンパクのようにプロテアーゼの活性を担う領域はなく，HBV pol がプロセスを受けて各ドメインに分解され，機能を発揮する可能性はないと考えられる[5) 9)]。

HBV は逆転写過程をもつ DNA ウイルスであり，逆転写過程をもつ RNA ウイルスであるレトロウイルスの生活環と根本的な違いがある。すなわち，レトロウイルスは感染後，細胞内侵入後に逆転写過程が始まり，最終的には2本鎖 DNA となり宿主染色体に組み込まれ，遺伝子発現，複製過程が進行する。

一方，HBV では感染後，転写産物として合成されたプレゲノム RNA を鋳型に粒子形成過程で逆転写が進行する。また，HBV の生活環には宿主染色体に組み込まれる過程は本質的にはない（感染肝細胞の増殖過程で非特異的に組み込みが起こることは知られており，初期段階ではレトロウイルスゲノムの末端部位の **LTR**〔long terminal region〕に相当する **DR**〔direct repeat〕が 5', 3' の両端に位置するほぼ完全な形で頻繁に組み込みが起こることが知られている）[10)]。

LTR (long terminal region)　**DR** (direct repeat)